









**Reversible Dispersion and Releasing of Single-Walled Carbon Nanotubes by  
Stimuli-Responsive TTFV-Phenylacetylene Polymers and Their Derivatives**

by

© Shuai Liang

A Thesis submitted to the

School of Graduate Studies

in partial fulfillment of the requirements for the degree of

**Master of Science**

**Department of Chemistry**

Memorial University of Newfoundland

**August 2012**

St. John's

Newfoundland

## Abstract

Carbon nanotubes (CNTs) have drawn considerable research attention owing to their unique properties and wide spectrum of applications in materials science. However, most applications of carbon nanotubes are still in preliminary stages due to the poor processibility of CNTs (*e.g.*, low solubility and strong aggregation). To overcome this barrier, a class of tetrathiafulvalene vinylogues (TTFV) and phenylacetylene based conjugated polymers were designed and investigated. The polymer backbone can reversibly fold and unfold under the control of redox and acid/base stimuli. This conformational switching property has allowed the polymer to reversibly disperse and release single-walled carbon nanotubes (SWNTs) in organic solvents in a controlled manner, which in turn opens a new avenue for recyclable and non-destructive SWNT processing techniques. In addition, a series of TTFV polymers with various side chains were synthesized for comparative studies to understand the effect of polymer structure on the supramolecular interaction with SWNTs.

## Acknowledgements

I would like to express my sincere appreciation to my supervisor, Prof. Yuming Zhao, for his generous help, constant encouragement, and tremendous guidance throughout my M.Sc. program.

Also, I would like to thank my co-supervisor, Prof. Wei Qiu, for his funding support, useful discussions and all other help throughout my study at Memorial University. I would like to extend my thanks to my supervisory committee member, Prof. Christopher Flinn, for spending time revising my thesis and his helpful suggestions for my projects.

I would like to thank Dr. Guang Chen for his tremendous help, training, and suggestions during my study. I also would like to extend my thanks to all my lab mates, especially Ph.D. student Mr. Karimulla Mulla for his helpful comments.

I am also thankful to all professors and staff in the Department of Chemistry at Memorial University, especially professors from the organic chemistry division, Prof. Graham Bodwell, Prof. Paris Georghiou and Prof. Sunil Pansare for their kind help during my study.

Last but not the least, I would like to express my appreciation to my family, especially my beloved wife, Jinghan Feng, for her endless love and support.

# Table of Contents

ABSTRACT.....	II
ACKNOWLEDGEMENTS.....	III
LIST OF TABLES.....	VIII
LIST OF FIGURES.....	IX
LIST OF SCHEMES.....	XIV
LIST OF SYMBOLS, NOMENCLATURE OR ABBREVIATIONS.....	XVI
CHAPTER 1 INTRODUCTION.....	1
1.1 A brief introduction to carbon nanotubes.....	1
1.2 Different strategies for noncovalent functionalization of SWNTs.....	7
1.2.1 Surfactants.....	8
1.2.2 Small aromatic molecules.....	9
1.2.3 Polymers.....	14
1.2.4 Block copolymers.....	28
1.2.5 Biomolecules.....	30
1.3 A Brief Introduction to tetrathiafulvalene vinylologues (TTFVs).....	31

1.4 Outline of this thesis .....	33
CHAPTER 2 SYNTHESIS AND CHARACTERIZATION OF TTFV POLYMERS AND TTFV POLYMER–SWNT COMPLEXES .....	36
2.1 Objectives of this project .....	36
2.2 Introduction to molecular design .....	37
2.3 Results and discussion .....	40
2.3.1 Synthesis of TTFV polymers .....	40
2.3.1.1 Synthesis of S-methyl thione 39 .....	40
2.3.1.2 Synthesis of S-methyl phosphonate 43 .....	41
2.3.1.3 Synthesis of tetrathiafulvalene vinylogues (TTFV) 46.....	42
2.3.1.4 Synthesis of aryl iodide 49.....	44
2.3.1.5 Synthesis of monomer 50 and TTFV polymer 51 .....	45
2.3.2 Characterization of TTFV polymer 51.....	47
2.3.2.1 Electronic and electrochemical properties of TTFV polymer 51. ....	49
2.3.2.2 UV-Vis titration experiments.....	52
2.3.2.3 AFM results of polymer 51 .....	58
2.3.2.4 SEM results of polymer film and acidified polymer film.....	62
2.3.3 Characterization of TTFV polymer –SWNTs complexes .....	68
2.3.3.1 UV-Vis-NIR results of TTFV polymer –SWNTs complexes.....	68
2.3.3.2 Raman spectroscopic results of TTFV polymer–SWNTs complexes .....	69

2.3.3.3 AFM results of CoMoCAT SWNTs-TTFV polymer complexes .....	70
2.3.3.4 SEM images and thermogravimetric analysis (TGA) of HiPCO SWNTs-TTFV polymer gel .....	72
2.3.3.5 Releasing of SWNTs from TTFV polymer-SWNTs complexes and multi-cycle dispersion-releasing of SWNTs .....	79
2.3.3.6 Procedure of multi-cycle dispersion-releasing of CoMoCAT SWNTs .....	82
2.2.3.7 Procedure of multi-cycle dispersion-releasing of HiPCO SWNTs .....	84
2.4 Summary .....	86
2.5 Experimental .....	86
 CHAPTER 3 SIDE-CHAIN EFFECT ON DISPERSION OF SWNTS WITH TTFV POLYMERS .....	 101
3.1 Objective of This Project .....	101
3.2.1 Synthesis of TTFV polymers 59 and 61 .....	102
3.2.1.1 Synthesis of aryl iodide 54 .....	102
3.2.1.2 Synthesis of aryl iodide 57 .....	103
3.2.1.3 Synthesis of monomer 58 and polymer 59 .....	103
3.2.1.4 Synthesis of monomer 60 and polymer 61 .....	105
3.2.2 Characterization of TTFV polymers 59 and 61 and their complexes with SWNTs .....	108
3.2.2.1 Electrochemical properties of polymers 59 and 61 .....	108

3.2.2.2 Characterization of TTFV polymers and SWNTs complexes .....	110
3.3 Summary .....	117
3.4 Experimental .....	118
CHAPTER 4 CONCLUSIONS AND FUTURE WORK .....	129

## List of Tables

<b>Table 2-1</b> Conditions that lead to the formation of HiPCO nanotube-TTFV polymer sol-gels in 1 mL of toluene. ....	73
<b>Table 2-2</b> Quantities of starting and recovered CoMoCAT SWNTs, polymer solution, and TFA used in the multi-cycle dispersion-releasing of SWNTs .....	83
<b>Table 2-3</b> Quantities of starting and recovered HiPCO SWNTs, polymer solution, and TFA used in the multi-cycle dispersion-releasing of SWNTs .....	96

## List of Figures

<b>Figure 1-1</b> Functionalization possibilities for SWNTs: A) defect-group functionalization, B) covalent sidewall functionalization, C) noncovalent exohedral functionalization with surfactants, D) noncovalent exohedral functionalization with polymers, and E) endohedral functionalization with, for example, $C_{60}$ . For methods B-E, the tubes are drawn in idealized fashion, but defects are found in real situations. ....	4
<b>Figure 1-2</b> Chemical structures of sodium dodecylsulfate <b>5</b> (SDS) and benzylalkonium chlorides <b>6</b> .....	8
<b>Figure 1-3</b> Chemical structure of <i>N</i> -succinimidyl-1-pyrenebutanoate <b>7</b> .....	9
<b>Figure 1-4</b> Chemical structure of trimethyl-(2-oxo-2-pyren-1-yl-ethyl)-ammonium bromide <b>8</b> .....	10
<b>Figure 1-5</b> Photoinduced cyclization of water-soluble stilbene <b>9</b> to form compound <b>10</b> .....	12
<b>Figure 1-6</b> Chemical structure of derivatized porphyrin <b>11</b> .....	13
<b>Figure 1-7</b> Chemical structure of ligand <b>12</b> .....	14
<b>Figure 1-8</b> Chemical structure of poly( <i>m</i> -phenylenevinylene)- <i>co</i> -(2,5-dioctoxy-phenylenevinylene) <b>13</b> (PmPV), poly(2,6-pyridinenevinylene)- <i>co</i> -(2,5-dioctoxy- <i>p</i> -phenylenevinylene) <b>14</b> (PPyPV), poly(5-alkoxy- <i>m</i> -phenylenevinylene)- <i>co</i> -(2,5-dioctoxy- <i>p</i> -phenylenevinylene) <b>15</b> (PAmPV).....	16
<b>Figure 1-9</b> Chemical structure of polyimides <b>16</b> .....	17
<b>Figure 1-10</b> Chemical structure of fluorescein-polyethylene glycol <b>17</b> .....	17
<b>Figure 1-11</b> Chemical structure of regioregular poly(3-alkylthiophene)s <b>18</b> .....	18

<b>Figure 1-12</b> Chemical structures of poly(9,9-dioctylfluorenyl-2,7-diyl) <b>19</b> (PFO) and poly [(9,9-dioctylfluorenyl-2,7-diyl)- <i>alt-co</i> -(1,4-benzo-2,10,3-thiadiazole)] <b>20</b> (PFO-BT)	19
<b>Figure 1-13</b> Chemical structure of poly[p-{2,5-bis(3- propoxysulfonic acid sodium salt) phenyleneethynylene} <b>21</b> (PPES)	21
<b>Figure 1-14</b> Chemical structures of poly(aryleneethynylene)s derivatives ( <b>22</b> and <b>23</b> )	22
<b>Figure 1-15</b> Chemical structures of poly (arylene ethynylene)s <b>25</b>	23
<b>Figure 1-16</b> Chemical structure of poly(vinylpyrrolidone) <b>26</b> (PVP) and polystyrene sulfonate <b>27</b> (PSS)	24
<b>Figure 1-17</b> Chemical structures of poly( <i>N</i> -isopropylacrylamide) <b>29</b> (PNIPAAm) and poly- <i>L</i> -lysine <b>30</b> (PLL)	26
<b>Figure 1-18</b> Chemical structure of poly(ethylene glycol)-terminated malachite green derivative (PEG-MG) <b>31</b>	27
<b>Figure 1-19</b> Chemical structure of poly(3-hexylthiophene)- $\beta$ -polystyrene <b>32</b>	28
<b>Figure 1-20</b> Chemical structures of copolymer of 9,9-bis( <i>n</i> -decyl)fluorine (F10) and 9,9-bis[( <i>S</i> )-(+)-2-methylbutyl]fluorine (F5) <b>33</b>	29
<b>Figure 1-21</b> Redox controlled conformation switching behavior of dipheny-TTFV	32
<b>Figure 2-1</b> Bistable conformational changes of TTFV under (a) redox and (b) acid/base conditions. (c) Reversible wrapping and unwrapping of SWNT by a TTFV polymer	38
<b>Figure 2-2</b> Structure of the designed folding TTFV polymer	39

<b>Figure 2-3</b> GPC chromatogram of TTFV polymer <b>51</b> . $M_n = 13400$ g/mol, $M_w = 51900$ g/mol, PDI = 3.9. Experimental conditions: columns: 2xPolyPore; standard: polystyrene; sample concentration: 1 mg polymer in 3 mL THF.....	48
<b>Figure 2-4</b> Optimized molecular structure of the hexamer of polymer <b>51</b> using the <i>SYBYL</i> force field implemented in Spartan <sup>®</sup> 10. ....	49
<b>Figure 2-5</b> (UV-Vis absorption spectra of compounds <b>46</b> , <b>50</b> , and <b>51</b> measured in toluene.....	50
<b>Figure 2-6</b> Cyclic voltammogram of TTFV <b>46</b> , monomer <b>50</b> , and polymer <b>51</b> . Experimental conditions: TTFV <b>46</b> ( $10^{-3}$ M), monomer <b>50</b> ( $10^{-3}$ M), and polymer <b>51</b> (2 mg/mL); $Bu_4NBF_4$ (0.1 M) as supporting electrolyte; $CH_2Cl_2$ as solvent; glassy carbon as working electrode; Pt wire as counter electrode; Ag/AgCl as reference; scan rate: 200 mv/s.....	51
<b>Figure 2-7</b> Protonation reactions of TTFV .....	53
<b>Figure 2-8</b> UV-Vis absorption spectra of TTFV <b>46</b> in $CH_2Cl_2$ upon addition of TFA from. (A) 0 to $1.6 \times 10^4$ equiv, and (B) $1.6 \times 10^4$ to $7.0 \times 10^4$ equiv. The arrows indicate the trends of spectral changes .....	54
<b>Figure 2-9</b> UV-Vis absorption spectra of monomer <b>50</b> in $CH_2Cl_2$ upon addition of TFA from. (A) 0 to $6.0 \times 10^4$ equiv, and (B) $6.0 \times 10^4$ to $1.0 \times 10^5$ equiv. The arrows indicate the trends of spectral changes .....	56
<b>Figure 2-10</b> UV-Vis absorption spectra of polymer <b>51</b> in $CH_2Cl_2$ upon addition of TFA from.(A) 0 to $2.0 \times 10^4$ equiv, and (B) $2.0 \times 10^4$ to $6.0 \times 10^4$ equiv (molar equiv was	

calculated based on the average molecular weight of polymer determined by GPC). The arrows indicate the trends of spectral changes.....	57
<b>Figure 2-11</b> AFM images of pure polymer <b>51</b> spin-coated on mica.....	59
<b>Figure 2-12</b> AFM images of acidified polymer <b>51</b> on mica.....	61
<b>Figure 2-13</b> Statistic counts of heights of pure polymer and acidified polymer.....	62
<b>Figure 2-14</b> Photograph of a thin film of polymer <b>51</b> .....	63
<b>Figure 2-15</b> SEM image of polymer film <b>51</b> .....	64
<b>Figure 2-16</b> Statistic count of diameter distribution of nano-discs on polymer film <b>51</b> ..	65
<b>Figure 2-17</b> Photograph of acidified polymer film <b>51</b> .....	66
<b>Figure 2-18</b> SEM image of acidified polymer film <b>51</b> .....	67
<b>Figure 2-19</b> UV-Vis-NIR spectra of SWNTs dispersed in toluene solution of polymer <b>5</b> .....	69
<b>Figure 2-20</b> The RBM region of Raman spectra ( $\lambda_{ex} = 534$ nm) for SWNTs dispersed by polymer <b>51</b> .....	70
<b>Figure 2-21</b> AFM image (tapping mode) of CoMoCAT SWNTs and polymer <b>51</b> on a mica surface.....	71
<b>Figure 2-22</b> Photographic images illustrating the bulky sol-gel formation resulting from ultrasonication of HiPCO nanotubes and polymers <b>51</b> in toluene.....	73
<b>Figure 2-23</b> SEM image of the gel film of HiPCO SWNTs and polymer <b>51</b> .....	74
<b>Figure 2-24</b> SEM image of diluted gel of HiPCO SWNTs and polymer <b>51</b> .....	75
<b>Figure 2-25</b> Schematics of polymer <b>51</b> induced stacking of HiPCO SWNTs.....	76
<b>Figure 2-26</b> Photograph of HiPCO SWNTs-polymer film.....	77

<b>Figure 2-27</b> Cyclic voltammogram of HiPCO SWNTs-polymer xerogel. Experimental conditions: Bu <sub>4</sub> NBF <sub>4</sub> (0.1 M) as supporting electrolyte; acetonitrile as solvent; HiPCO SWNTs-polymer film as working electrode; Pt wire as counter electrode; Ag/AgCl as reference; scan rate: 100 mv/s.....	64
<b>Figure 2-28</b> TGA of polymer film and HiPCO SWNTs-polymer film under N <sub>2</sub> .....	65
<b>Figure 2-29</b> Schematics of multi-cycle dispersion–releasing of SWNTs in toluene solution of polymer <b>51</b> .....	80
<b>Figure 2-30</b> (A) UV-Vis-NIR absorption spectra monitoring multi-cycle dispersion of CoMoCAT SWNTs. (B) UV-Vis-NIR absorption spectra monitoring multi-cycle dispersion of HiPCO SWNTs .....	81
<b>Figure 2-19</b> UV-Vis-NIR spectra of SWNTs dispersed in toluene solution of polymer <b>5</b> .....	69
<b>Figure 2-20</b> The RBM region of Raman spectra ( $\lambda_{ex} = 534$ nm) for SWNTs dispersed by polymer <b>51</b> .....	70
<b>Scheme 3-1</b> Synthesis of aryl iodide <b>54</b> .....	102
<b>Scheme 3-2</b> Synthesis of aryl iodide <b>57</b> .....	103
<b>Scheme 3-3</b> Synthesis of monomer <b>58</b> and TTFV polymer <b>59</b> .....	105
<b>Scheme 3-4</b> Synthesis of monomer <b>60</b> and TTFV polymer <b>61</b> .....	107

## List of Schemes

<b>Scheme 1-1</b> Synthesis of TTF- and exTTF-functionalized SWNTs .....	6
<b>Scheme 1-2</b> 1-Pyrenebutanoic acid succinimidyl ester <b>7</b> irreversibly adsorbed onto the sidewall of a SWNT via $\pi$ -stacking.....	10
<b>Scheme 1-3</b> Schematic diagram of dispersibility change of SWNTs by photoinduced structural change of the dispersan.....	12
<b>Scheme 1-4</b> Molecular modeling showing radial views of three nanotube species encased with PFO chains of six repeat units in length with the polymer backbone coloured in blue and the side chains in yellow .....	20
<b>Scheme 1-5</b> Solution process for dispersion and release of SWNTs by mPE-13mers <b>28</b> .....	25
<b>Scheme 1-6</b> Mechanism for oxidative dimerization of aryl-DTF to form diaryl-TTFV..	33
<b>Scheme 2-1</b> Synthesis of <i>S</i> -methyl thione <b>39</b> .....	40
<b>Scheme 2-2</b> Synthesis of <i>S</i> -methyl phosphonate <b>43</b> .....	41
<b>Scheme 2-3</b> Synthesis of aldehyde <b>44</b> .....	42
<b>Scheme 2-4</b> Synthesis of dithiafulvene alkyne <b>45</b> .....	42
<b>Scheme 2-5</b> Alternative synthetic route to dithiafulvene alkyne <b>45</b> .....	43
<b>Scheme 2-6</b> Synthesis of phenylacetylene-substituted TTFVs <b>46</b> .....	44
<b>Scheme 2-7</b> Synthesis of aryl iodide <b>49</b> .....	45
<b>Scheme 2-8</b> Synthesis of monomer <b>50</b> and TTFV polymer <b>51</b> .....	46
<b>Scheme 3-1</b> Synthesis of aryl iodide <b>54</b> .....	102
<b>Scheme 3-2</b> Synthesis of aryl iodide <b>57</b> .....	103

<b>Scheme 3-3</b> Synthesis of monomer <b>58</b> and TTFV polymer <b>59</b> .....	105
<b>Scheme 3-4</b> Synthesis of monomer <b>60</b> and TTFV polymer <b>61</b> .....	107

## List of Symbols and Abbreviations

$\delta$	chemical shift
AFM	atomic force microscopy
aq	aqueous
Bu	butyl
conc	concentrated
CoMoCAT	cobalt-molybdenum catalyzed
CNTs	carbon nanotubes
calcd	calculated
CV	Cyclic voltammetry
d	deuterium (in NMR solvent, e.g. THF-d8)
d	doublet
DBU	1,8-diazabicyclo[5.4.0]undec-7-ene
DMF	N,N-dimethylformamide
Epa	potential of anodic peak
Epc	potential of cathodic peak
eq.	equivalents
Et <sub>3</sub> N	triethylamine
FET	field effect transistor
FTIR	fourier transform Infrared (spectroscopy)
g	gram(s)
GPa	gigapascal

h	hour(s)
HiPCO	high pressure CO disproportionation
IR	infrared (spectroscopy)
J	(in NMR) coupling constant (Hz)
LED	light emitting diode
LUMO	lowest unoccupied molecular orbital
m	multiplet
m/z	mass to charge ratio
HOMO	highest occupied molecular orbital
MALDI-TOF	matrix assisted laser desorption/ionization–time of flight
Me	methyl
mg	milligram(s)
MHz	megahertz
min	minute(s)
M <sup>+</sup>	mass peak
Me	methyl, CH <sub>3</sub>
mL	milliliter(s)
MeCN	acetonitrile
mmol	millimole(s)
mol	mole(s)
MWNT	multi-walled nanotube
nm	nanometer

NMR	nuclear magnetic resonance (spectroscopy)
p	para
Ph	phenyl
ppm	parts per million
Q	quartet (in NMR)
rt	room temperature
s	second(s) or singlet
SDS	dodecylsulfonate
SWNT	single-walled nanotube
t	triplet
TFA	trifluoroacetic acid
THF	tetrahydrofuran
TLC	thin layer chromatography
TMS	trimethylsilyl
TMSA	trimethylsilylacetylene
TPa	terapascal
TTFV	tetrathiafulvalene vinylogue
UV-Vis	ultraviolet-visible
UV-Vis-NIR	ultraviolet-visible-near infrared (spectroscopy)
V	volt(s)

# Chapter 1

## Introduction

### 1.1 A brief introduction to carbon nanotubes

Carbon nanotubes (CNTs), since their first discovery<sup>1</sup> in 1991 by Iijima and co-workers, have drawn enormous research attention because of their unique structural, electrical, optical, thermal, and mechanical properties. CNTs have remarkable mechanical properties such as elastic modulus and strengths 10–100 times higher than the strongest steel at a fraction of the weight.<sup>2</sup> In 2000, Yu *et al.* measured the Young's moduli of individual multi-walled nanotubes (MWNT) to be between 0.27–0.95 TPa, with strengths in the 11–63 GPa range, and toughness of  $\sim 1240 \text{ J g}^{-1}$ .<sup>3</sup> For single-walled nanotubes (SWNT), the mechanical properties appear to be even better; their Young's moduli were found to be in the range of 0.32–1.47 TPa and strengths between 10 and 52 GPa with toughness of  $\sim 770 \text{ J g}^{-1}$ .<sup>4</sup> CNTs also exhibit unique electrical properties and electric-current-carrying capacity 1000 times higher than copper wire.<sup>4</sup> Frank *et al.* calculated the conductance of an average nanotube to be  $1/12.9 \text{ k}\Omega^{-1}$ .<sup>5</sup> These extraordinary properties have led to very promising applications ranging from photovoltaic devices, field-effect transistors to advanced composite materials.<sup>6</sup> For example, individual SWNT based field-effect transistors (FETs) have been fabricated and characterized to show excellent performance over current silicon-based complementary metal oxide semiconductor (CMOS) devices.<sup>7</sup>

SWNTs can be prepared by various methods.<sup>8</sup> The first synthesis of SWNTs was achieved by arc discharge of graphite in the presence of metal catalysts (e.g., Fe, Co, and Ni). Although this method is cheap and easy to implement, it suffers from the significant shortcoming of very low yields.<sup>9</sup> Later on, methods based on laser vaporization of graphite-nickel-cobalt mixtures or chemical vapor deposition (CVD) were invented, in which various carbon sources such as acetylene, metallocenes,  $\text{Fe}(\text{CO})_5/\text{C}_2\text{H}_2$ , and CO were used.<sup>9</sup> One remarkable example of CNT syntheses is the high pressure CO disproportionation process (HiPCO) developed by Prof. Richard Smalley's group at Rice University, using CO as carbon source and  $\text{Fe}(\text{CO})_5$  as catalyst in a continuous flow gas phase. This method has become a widely used technique for catalytic production of SWNTs, by which very thin nanotubes can be produced in large quantity within a matter of hours,<sup>10</sup> and the products contain up to 70% of SWNTs by mass. Recently, Prof. Daniel Resasco's group developed the production method for the so-called CoMoCAT nanotubes using CO disproportionation (decomposition into C and  $\text{CO}_2$ ) at 700-950°C to grow SWNTs with a narrow distribution of tube diameters. The advantage of this technique lies in the usage of a unique cobalt-molybdenum (Co-Mo) catalyst formulation that inhibits the sintering of Co particles and therefore avoids the formation of undesired forms of carbon.

Conceptually, SWNTs can be described as a graphene sheet rolled into a cylindrical nanostructure with hemispherical fullerene caps at both ends. Usually, they are generated by the action of a metal catalyst on carbon vapor at high temperature. The wrapping of

the graphene sheet can occur in many different ways leading to many distinct possible SWNTs structures such as “zigzag”, “armchair”, and “chiral”. The physical properties of SWNTs are strongly dependent on the structures defined by the chiral indices  $n$  and  $m$ .<sup>11</sup> If  $n = m$ , SWNTs are named armchair; if  $m = 0$ , they are zigzag; in other situations they are chiral. In terms of electronic types, there are two types of SWNTs, metallic and semiconducting nanotubes. If  $n - m = 3x$  (where  $x$  is an integer), SWNTs are metallic, otherwise they are semiconducting.

So far all known growth methods generate SWNT samples with a broad distribution of chiral indices and each structure is characterized by its diameter and the angle of its graphene lattice to the nanotube axis. Therefore, as-produced SWNTs are not homogeneous. This property limits most applications of SWNTs to the preliminary stage. To find a way to sort out and enrich SWNTs into distinct species or electronic types (*e.g.*, metallic versus semiconducting) has become an important topic of research. In addition, pristine SWNTs strongly bundle together due to strong van der Waals intertube attraction, causing severe aggregation which impairs the unique and intrinsic properties of individual nanotubes and weakens their performance when employed in devices. Methods to solubilize and disperse SWNTs in organic solvents and aqueous media are needed to overcome this barrier. Effective dispersion of SWNTs can also facilitate purification of SWNTs, since as-produced nanotubes are invariably contaminated with impurities such as metal catalyst particles, amorphous carbon, and other carbonaceous species.

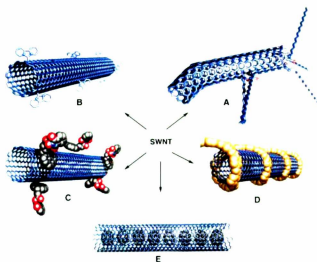
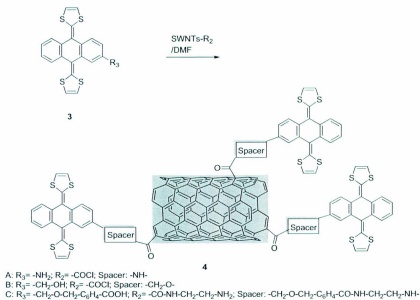
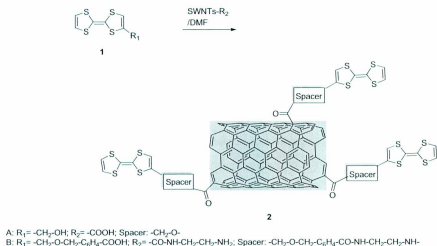


**Figure 1-1.** Functionalization possibilities for SWNTs: A) defect-group functionalization, B) covalent sidewall functionalization, C) noncovalent exohedral functionalization with surfactants, D) noncovalent exohedral functionalization with polymers, and E) endohedral functionalization with, for example, C<sub>60</sub>. For methods B-E, the tubes are drawn in idealized fashion, but defects are found in real situations (adopted from reference 8 with permission).

To date, numerous methods for SWNT functionalization have been developed through both molecular and supramolecular approaches. These approaches include defect functionalization, covalent functionalization of the sidewalls, noncovalent exohedral functionalization, and endohedral functionalization as summarized in Figure 1-1.<sup>8</sup> However, for the purpose of dispersion and purification, covalent and noncovalent

functionalization taking place at the sidewall of SWNTs appear to be very effective. Covalent methods are able to flexibly introduce a variety of chemical moieties on the surface of SWNTs to tailor the properties of the nanotube surface. Covalent functionalizations of SWNTs can also cope with some problems with respect to purification, solubilization, and processing.<sup>3</sup> For example, treatment of nanotubes in HNO<sub>3</sub> oxidizes the surface and introduces oxygenated groups such as carboxylic acid groups onto the tips and defect sites of nanotube surfaces. Such chemical reactions cause the nanotubes to be cut into shorter “pipes” and substantially improve their solubility in organic solvents<sup>12</sup> and even in water<sup>13</sup>, thereby leading to a stable dispersion of these materials.<sup>14</sup> Furthermore, covalent functionalization can greatly alter the intrinsic properties of SWNTs. For instance, Scheme 1-1 shows tetrathiafulvalenes (TTFs) and/or  $\pi$ -extended tetrathiafulvalenes (exTTFs) acting as electron donors to be covalently tethered to SWNTs by an esterification reaction. In this system, control over rate of electron transfer was gained by either systematically altering the relative donor–acceptor separations or by integrating different electron donors.<sup>15</sup>



**Scheme 1-I.** Synthesis of TTF- and exTTF-functionalized SWNTs.

On the other hand, the covalent approach has drawbacks. The chemical reactions on the side walls of the SWNTs with functionalizing groups cause undesirable disruption of the electronic and/or mechanical properties of SWNTs.<sup>14</sup> Noncovalent methods, in contrast, are typically conducted through surface binding of surfactants<sup>8,16</sup> or adhesion of small molecules<sup>17-21</sup>, or wrapping with polymers<sup>22-38</sup> or biomolecules<sup>39-41</sup>, hence showing obvious advantages over covalent methods. Instead of dramatically changing the intrinsic properties of the SWNTs, as often occurs when covalent methods are used, the noncovalent methods alter the properties of the SWNTs only to a slight or moderate degree. In the following section, noncovalent functionalization of SWNTs will be elaborated in detail as it is pertinent to the work of this thesis.

## **1.2 Different strategies for noncovalent functionalization of SWNTs**

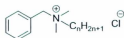
SWNTs can interact with a large variety of molecules and macromolecules noncovalently, resulting in debundling of the aggregated tubes and forming supramolecular complexes with significantly improved solubility in various solvents. As such, SWNTs can be effectively dissolved or dispersed in solvents to facilitate further processing and modification. In the literature, there is a plethora of noncovalent methods reported and this section gives a general overview of them. The review herein is organized according to the type of molecules or macromolecules used as SWNT dispersants, ranging from surfactants, small molecules, polymers, copolymers and biomolecules. Because of the significant relevance to this thesis work, methods employing polymers as SWNT dispersants will be elaborated on with particular emphasis.

### 1.2.1 Surfactants

In the search for nondestructive dispersion methods, surfactant-assisted dispersion has been an easy and effective technique to transfer nanotubes into the aqueous phase. Commonly used surfactants for nanotube dispersion are sodium dodecylsulfate **5** (SDS)<sup>16</sup> and benzylalkonium chlorides **6**<sup>8</sup> (see Figure 1-2). It is believed that when interacting with surfactants nanotubes are encapsulated in the hydrophobic interiors of the micelles formed by these surfactant molecules to yield stable dispersion. When the hydrophobic parts of the surfactant molecules contain aromatic groups,  $\pi$ - $\pi$  interactions between the aryl moieties and the graphitic sidewalls of nanotubes can result in effective coating and dispersion.<sup>8</sup>



**5**



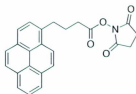
n = 8, 10, 12, 14, 16, 18

**6**

**Figure 1-2.** Chemical structures of sodium dodecylsulfate **5** (SDS) and benzyltrialkylammonium chlorides **6**.

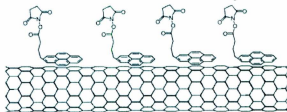
### 1.2.2 Small aromatic molecules

1-Pyrenebutanoic acid succinimidyl ester **7** (Figure 1-3) was found to irreversibly adsorb onto the inherently hydrophobic surfaces of SWNTs in an organic solvent such as dimethylformamide (DMF) or methanol. The pyrenyl group, being aromatic in nature, is known to interact strongly with the basal plane of graphite via  $\pi$ -stacking, and to strongly adhere to the sidewalls of SWNTs in a similar manner. Interestingly, since the *N*-hydroxysuccinimide groups attached to SWNTs are highly reactive to nucleophilic substitution by primary and secondary amines that exist in abundance on the surface of most proteins, it is possible to link proteins such as ferritin, streptavidin, and biotiny-3,6-dioxaoctanediamine onto these pyrenyl succinimide functionalized nanotubes (Scheme 1-2).<sup>17</sup> This property could be used in the development of biosensors that operate based on the change of the electronic properties of SWNTs in response to the binding events taking place at the immobilized bio-receptor systems attached.<sup>8</sup>



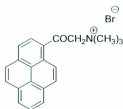
**7**

**Figure 1-3.** Chemical structure of *N*-succinimidyl-1-pyrenebutanoate **7**.



**Scheme 1-2.** 1-Pyrenebutanoic acid succinimidyl ester **7** irreversibly adsorbed onto the sidewall of a SWNT via  $\pi$ -stacking (adopted from reference 17 with permission).

Apart from dispersion in organic solvents, small aromatics based dispersants have also been utilized to disperse SWNTs in the aqueous phase. For example, a pyrene-carrying ammonium ion, trimethyl-(2-oxo-2-pyren-1-yl-ethyl)-ammonium bromide **8** (Figure 1-4) was designed and synthesized as a dispersant to solubilize SWNTs in water. The  $\pi$ -stacking of the pyrene moiety with the sidewall of the nanotube plays a significant role in imparting water solubility to SWNTs.<sup>18</sup>



**8**

**Figure 1-4.** Chemical structure of trimethyl-(2-oxo-2-pyren-1-yl-ethyl)-ammonium bromide **8**.

A water-soluble stilbene **9** (Figure 1-5) was reported by Yoko Matsuzawa *et al.* to be the first example of a low-molecular-weight dispersant giving a high efficiency of dispersing SWNTs in water with an on-off tunable property upon photoirradiation. Compound **9** has a photoactive electrolyte with stilbene as the photoresponsive core and a tetraalkylammonium unit at the termini as the water solubilizing group. *Trans*-stilbene **9** can transform into phenanthrene **10** in good yield via a photocyclization reaction in the presence of a suitable oxidant such as the dissolved molecular oxygen in solution. Based on density functional theory (DFT) calculations, the cationic part of compound **9** adopts a conformation where the central stilbene is coplanar with the benzamide units. The resulting planar  $\pi$ -surface of **9** can interact with SWNTs via strong  $\pi$ -stacking leading to effective dispersion of SWNTs. After photocyclization, the cationic part of the photocyclized product **10** takes a highly twisted and bent structure that disfavors the  $\pi$ - $\pi$  interaction with SWNTs.<sup>19</sup> As such, stilbene **9** and SWNT complexes can be readily dissociated under the irradiation of UV light to release pristine SWNTs (see Scheme 1-3).<sup>19</sup>

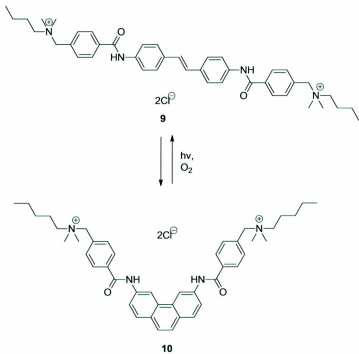
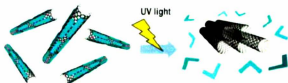


**Figure 1-5.** Photoinduced cyclization of water-soluble stilbene **9** to form compound **10**.



**Scheme 1-3.** Schematic diagram of dispersibility change of SWNTs by photoinduced structural change of the dispersant (adopted from reference 19 with permission).

The separation and enrichment of a specific electronic type of SWNTs from a mixture of SWNTs has been achieved using small aromatic molecules. For example, Yaping Sun *et al.* reported that derivatized porphyrins **11** (Figure I-6) showed good selectivity toward semiconducting SWNTs by noncovalent interactions. Upon interaction with a mixture of SWNTs, semiconducting SWNTs were significantly enriched in the solubilized portion, whereas the insoluble residual solid consisted predominantly of metallic SWNTs according to Raman, near-IR absorption, and bulk conductivity characterizations. To explain this behavior, the authors proposed that the semiconducting and metallic SWNTs have very different surface properties. A semiconducting SWNT behaves more like a conjugated macromolecule and preferentially binds with the free-base porphyrin in a manner similar to those found in radical ion pairs.<sup>20</sup>

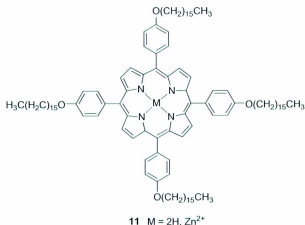


**Figure I-6.** Chemical structure of derivatized porphyrin **11**.

A planar  $\text{Cu}^{\text{II}}$  complex has been reported as a solubilizing agent to disperse SWNTs in organic solvents. The ligand of the complex is a 2,2'-bipyridine core appended with two cholesteryl groups (see **12** in Figure 1-7). Upon reduction of the central metal atom, the ligand changes from a planar to a nonplanar structure, causing the dissociation of the metal complexes and releasing of the dispersed SWNTs due to the disappearance of  $\pi$ -stacking between the  $\pi$ -conjugated planar molecule and the SWNT surfaces. In this way, the dispersion process can be controlled by changing the redox state of the  $\text{Cu}^{\text{I}}/\text{Cu}^{\text{II}}$  complexes via chemical oxidation and reduction.<sup>21</sup>

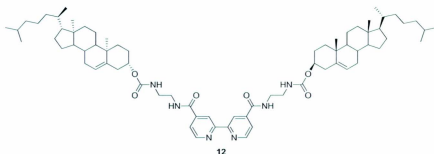


**Figure 1-7.** Chemical structure of ligand **12**.

### 1.2.3 Polymers

Polymers have been extensively used in the formation of supramolecular complexes with SWNTs to disperse SWNTs in common organic solvents or even in aqueous media. Polymers, especially  $\pi$ -conjugated polymers, have the ability to wrap themselves around

SWNTs as a result of  $\pi$ -stacking and van der Waals interactions between the conjugated polymers and the surfaces of SWNTs.

James R. Heath *et al.* reported the use of a series of conjugated polymers (Figure 1-8), including poly(*m*-phenylenevinylene)-*co*-(2,5-dioctoxy-phenylenevinylene) **13** (PmPV),<sup>22</sup> poly(2,6-pyridinlenevinylene)-*co*-(2,5-dioctoxy-*p*-phenylenevinylene) **14** (PPyPV),<sup>23</sup> poly(5-alkoxy-*m*-phenylenevinylene)-*co*-(2,5-dioctoxy-*p*-phenylenevinylene) **15** (PAmPV)<sup>24</sup> to disperse SWNTs in organic solvents. The authors claimed that these polymers wrapped around bundles of the SWNTs rather than individual tubes, which then aggregated to form ropes. Since SWNTs are ideal candidates as bridges across microelectrodes for charge-transport measurements due to their high aspect ratios, the polymers/SWNTs hybrids can be useful in fabricating nanoscale electronic devices. For example, PmPV-wrapped SWNTs show on/off switching properties for negatively and positively biased junctions. The magnitude of the change in current corresponds to *ca.* 15-20% of the total current. The electric current passing through the PmPV/SWNT device is photo-amplified for a positive applied bias but is photorectified for a negative one.<sup>25</sup>

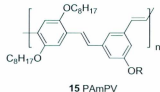
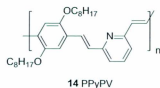
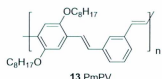
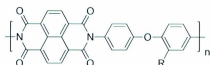


**Figure 1-8.** Chemical structure of poly(*m*-phenylenevinylene)-*co*-(2,5-dioctoxy-phenylenevinylene) **13** (PmPV), poly(2,6-pyridinenevinylene)-*co*-(2,5-dioctoxy-*p*-phenylenevinylene) **14** (PPyPV), poly(5-alkoxy-*m*-phenylenevinylene)-*co*-(2,5-dioctoxy-*p*-phenylenevinylene) **15** (PAmpV).

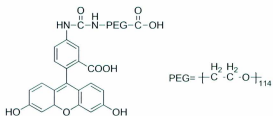
Naotoshi Nakashima *et al.* reported that polyimide derivatives **16** (Figure 1-9) were able to selectively disperse SWNTs with (7, 6), (7, 5), (8, 4), (9, 5) and (8, 6) indices in organic solvents. With increasing concentrations of SWNTs, the solutions became viscous and then changed into gels. They explained that the condensed aromatic moieties on polyimide induced significant interactions with the surface of SWNTs.<sup>26</sup>



16

**Figure I-9.** Chemical structure of polyimides **16**.

Dai *et al.* reported the noncovalent functionalization of SWNTs using fluorescein-polyethylene glycol **17** (Fluor-PEG, Figure I-10) to impart aqueous solubility with simultaneous fluorescent labeling to nanotubes. Interestingly, the optical absorbance and fluorescence of fluorescein bound to SWNTs are distinctly different from those of free fluorescein, and the binding of Fluor-PEG with SWNTs is pH-dependent. The results are important for understanding of supramolecular chemistry of nanomaterials and point to potential applications such as pH sensing.<sup>27</sup>



17

**Figure I-10.** Chemical structure of fluorescein-polyethylene glycol **17**.

Selective enrichment of different electronic types of SWNTs, such as semiconducting or metallic SWNTs, is highly desirable for device applications. Bao *et al.* reported that regioregular poly(3-alkylthiophene)s (rr-P3ATs) could be used to selectively disperse semiconducting SWNTs (sc-SWNTs). Their study showed that rr-P3ATs with longer alkyl side chains ( $-C_{12}H_{25}$ ) are able to disperse a higher percentage of SWNTs, as compared with other rr-P3ATs with smaller side chains. They also reported that the temperature used during the sonication is another important parameter. The highest absorption intensity for rr-P3ATs is observed when dispersion is conducted at 50 °C (studied from -40 to 90 °C). This temperature coincides with the melting point of the side chains of rr-P3ATs. Based on molecular modeling studies, a supramolecular structure consisting of two polymer strands wrapped around SWNTs with side chains interdigitated was proposed to explain the experimental results. Moreover, a thin-film transistor was fabricated using sorted semiconducting SWNTs to exhibit an excellent charge-carrier mobility as high as  $12 \text{ cm}^2 \text{ V}^{-1} \text{ S}^{-1}$  and on/off ratio of  $>10^6$ .<sup>28</sup>

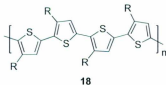


**Figure I-11.** Chemical structure of regioregular poly(3-alkylthiophene)s **18**.

Robin J. Nicholas *et al.* have demonstrated that fluorene-based conjugated polymers could selectively solubilize certain nanotube species depending on chiral angle and

nanotube diameter. The distribution of solubilized nanotube species has a strong dependence on the polymer structure. Minor change of polymer side chains and backbone has a significant effect on the number of species that are solubilized. The most remarkable selectivity is seen using the poly(9,9-dioctylfluorenyl-2,7-diyl) (PFO) and poly[(9,9-dioctylfluorenyl-2,7-diyl)-*alt-co*-(1,4-benzo-2,10,3-thiadiazole)] (PFO-BT). It was found that for HiPco SWNTs, only six species can be detected in the PFO/SWNTs solutions, all with a very strong chiral angle bias, because all of the observed SWNTs are close to the armchair configuration. For the PFO-BT/SWNTs solution, nine species are detected, with a strong selectivity for nanotubes with diameters around 1.05 nm. More interestingly, for CoMoCAT SWNTs, it was found that the strong selectivity of PFO resulted in around 60% of all the suspended tubes being the (7,5) species, without any trace of the formerly dominant (6,5) tubes.<sup>29</sup>

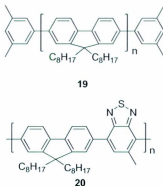
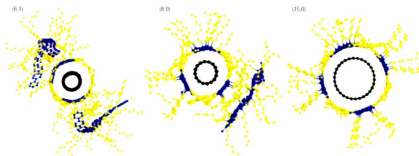
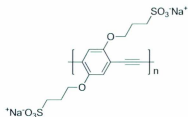


**Figure 1-12.** Chemical structures of poly(9,9-dioctylfluorenyl-2,7-diyl) **19** (PFO) and poly [(9,9-dioctylfluorenyl-2,7-diyl)-*alt-co*-(1,4-benzo-2,10,3-thiadiazole)] **20** (PFO-BT).



**Scheme 1-4.** Molecular modeling showing radial views of three nanotube species encased with PFO chains of six repeat units in length with the polymer backbone coloured in blue and the side chains in yellow (adopted from reference 28 with permission).

Michael J. Therien *et al.* reported that linear conjugated poly[*p*-{2,5-bis (3-propoxysulfonic acid sodium salt)}phenyleneethynylene] **21** (PPES) could be used to efficiently disperse SWNTs into the aqueous phase. PPES **21** is an amphiphilic polyelectrolyte consisting of a linear conjugated PPE backbone and two negatively charged side groups for every phenyl unit. The substantial  $\pi$ - $\pi$  interactions between PPES and SWNTs are provided by the aryeneethynylene repeat unit. It has been demonstrated that these solubilized SWNTs are highly individualized, as evidenced by UV-Vis-NIR, AFM and TEM analyses. Moreover, AFM and TEM data revealed that the interaction of PPES with SWNTs lead to a self-assembled superstructure in which a polymer monolayer helically wraps around the nanotube.<sup>30</sup>



21

**Figure 1-13.** Chemical structure of poly[p-(2,5-bis(3-propoxysulfonic acid sodium salt)phenyleneethynylene] **21** (PPE).

Walker *et al.* reported that short, rigid conjugated polymers, poly(aryleneethynylene) derivatives (compounds **23** and **24**, Figure 1-14) could solubilize SWNTs. In contrast to many other examples of polymer dispersants in the literature, the rigid backbone of PPE cannot wrap around SWNTs. The major interaction between the polymer backbone and the nanotube surface is most likely  $\pi$ -stacking. This approach represents the first example of CNT solubilization via  $\pi$ -stacking without polymer wrapping and enables the introduction of various neutral and ionic functional groups onto the CNT surface. In addition, Walker *et al.* claimed that the polymer wrapping approach worked poorly for dissolution of small-diameter SWNTs (the solubility of HiPCO SWNTs is about 0.1 mg/mL, using PmPV), possibly due to an unfavorable polymer conformation required for PmPV to wrap around small-diameter HiPCO SWNTs (diameter 0.7-0.8 nm). On the contrary, the more rigid **22A** can solubilize small-diameter HiPCO SWNTs at 2 mg/mL in  $\text{CHCl}_3$ .<sup>31</sup>

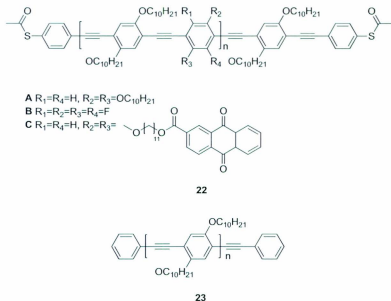
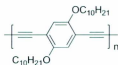


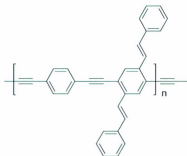
**Figure 1-14.** Chemical structures of poly(aryleneethynylene)s derivatives (**22** and **23**).

In the Zhao group, structurally rigid non-helical conjugated polymers, poly(arylene ethynylene)s, have also been designed and synthesized to disperse SWNTs in organic solvents, driven by strong  $\pi$ -stacking forces between conjugated polymers and SWNTs. The rigid backbones of these polymers were decorated with long *n*-decyloxy chains for two reasons: (i) to impart solubility in organic solvents, and (ii) to stabilize SWNT dispersions by steric repulsion. As a result, linear conjugated polymers, upon rational backbone modifications, can form stable and soluble supramolecular assemblies with as-prepared SWNTs powders in organic solutions via a surface coating mechanism. The

satisfactory dispersing and debundling results of polymers **24** and **25** indicate that this type of polymer serves as a novel generic platform for polymer-based SWNT dispersants.<sup>32</sup>



**24**



**25**

**Figure 1-15.** Chemical structures of poly(arylene ethynylene)s **25**.

Smalley *et al.* reported that polymers such as poly(vinylpyrrolidone) **26** (PVP) and polystyrene sulfonate **27** (PSS) (Figure 1-16) could disperse SWNTs in aqueous solutions through noncovalent wrapping, and the SWNT-polymer complexes could be reversibly unwrapped by changing the solvent system. They proposed that the wrapping of SWNTs by water-soluble polymers is dictated by a thermodynamic driving force to eliminate the

hydrophobic interface between SWNTs and the aqueous medium. Changing the solvent system to reduce the hydrophobic effect induces the dissociation of the PVP-SWNT complexes.<sup>33</sup>

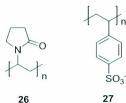
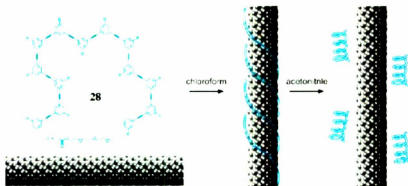


**Figure I-16.** Chemical structure of poly(vinylpyrrolidone) **26** (PVP) and polystyrene sulfonate **27** (PSS).

Moore *et al.* reported a simple, reversible route for dispersion and release of SWNTs involving the use of a particular kind of foldable oligomers (designated as foldamers), oligo(*m*-phenyleneethynylene)s **28** (mPE-13mers), simply by controlling their conformational states in different solvents. The folding of oligomer **28** is primarily controlled by the  $\pi$ - $\pi$  interaction between nonadjacent monomer units in conjunction with the solvophobic interaction between the hydrophobic backbone of the oligomer and solvent molecules. Therefore, mPE-13mers can effectively disperse SWNTs in the unfolded state in a nonpolar solvent such as chloroform. When the solvent is changed into a polar one, the mPE-13mers become folded and are conformationally disfavored for interfacial  $\pi$ - $\pi$  interactions with the nanotubes. As a result of the conformational change of the polymer, the bare nanotubes are released as a precipitate into the solvent. The

released SWNTs were used to fabricate field-effect transistors (FETs). The result shows that the released SWNTs are free of mPE-13mers.<sup>34</sup>



**Scheme 1-5.** Solution process for dispersion and release of SWNTs by mPE-13mers **28** (adopted from reference 33 with permission).

Temperature and pH-responsive polymers such as poly(*N*-isopropylacrylamide) **29** (PNIPAAm) and poly-*L*-lysine **30** (PLL) (Figure 1-17) have been used by Chen *et al.* to reversibly disperse and release SWNTs. The hydrocarbon main chain and the isopropyl side chains of PNIPAAm can interact with SWNT sidewalls through nonspecific van der Waals and hydrophobic interactions, while the hydrophilic amide bonds maintain the water solubility of PNIPAAm-SWNT complexes. The C=O and N-H groups of PNIPAAm can form intermolecular hydrogen bonds with surrounding water molecules. This bonding motif results in a gain in enthalpy, but pays an entropic price for limiting the motion of bound water molecules. Alternatively, the C=O and N-H groups can form

intramolecular hydrogen bonds themselves, which is less exothermic than the intermolecular H-bonding scenario but entropically favored for releasing water. In this case, the critical solution temperature (*i.e.*, LCST) is a key factor influencing the interactions between SWNTs and the polymers. LCST refers to the temperature below which the components of a mixture are miscible for all compositions. The LCST for PNIPAAm is around 33 °C. The equilibrium shifts toward the enthalpically favored intermolecular H-bonding conformation, whereas at temperatures above the LCST the equilibrium moves toward the entropically favored intramolecular H-bonding structure. This structural transition leads to reversible dispersion and releasing of SWNTs in aqueous media. In addition, uncharged PLL adopts a helical conformation at high pH, but adopts an uncoiled conformation in acidic or neutral pH due to the electrostatic repulsion among side-chain cations. The hydrocarbon linker moieties in the uncoiled PLL are more accessible to SWNTs. This property leads to the dispersion of SWNTs at acidic or neutral pH and release of SWNTs at high pH for PLL.<sup>35</sup>

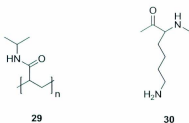
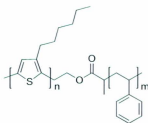


**Figure 1-17.** Chemical structures of poly(*N*-isopropylacrylamide) **29** (PNIPAAm) and poly-*L*-lysine **30** (PLL).



### 1.2.4 Block copolymers

A copolymer with a conjugated polymer block and a non-conjugated polymer block, poly(3-hexylthiophene)- $\beta$ -polystyrene **32** (P3HT- $\beta$ -PS) (Figure 1-19), has been reported to act as an excellent dispersant for CNT dispersion. Conjugated polymer blocks such as polythiophenes can strongly interact with CNT walls via  $\pi$ -stacking, while the non-conjugated polymer blocks provide the debundled CNTs with good solubility and stability in a wide range of organic solvents and host polymer matrices. Both SWNTs and MWNTs were well dispersed in chloroform by P3HT- $\beta$ -PS with gentle sonication. The highest CNT concentration of stable CNT dispersions is around 2.5 mg mL<sup>-1</sup> and 3.0 mg mL<sup>-1</sup> for SWNTs.<sup>37</sup>

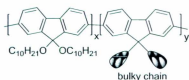


**32**

**Figure 1-19.** Chemical structure of poly(3-hexylthiophene)- $\beta$ -polystyrene **32**.

It has been reported that the chiral fluorine-based copolymer **33** (Figure 1-20), composed of 9,9-bis(*n*-decyl)fluorene (F10) and 9,9-bis[(*S*)-(+)-2-methylbutyl]fluorene (F5), can specifically recognize certain chiralities of semiconducting SWNTs, leading to selective

extraction of chiral SWNTs. PF-based copolymers are composed of a fluorene having two less-bulky, long achiral alkyl side chains to solubilize specific semiconducting SWNTs and a fluorene carrying two bulky, short chiral alkyl side chains, which can continuously alter the degree of helical wrapping ability onto the curved surface of the SWNT to achieve chirality recognition/solubilization ability by steric hindrance. This study has shown that copolymers with different  $x/y$  ratio can result in recognition of different chiralities of SWNTs. For instance, for the (7,5), (7,6), and (8,6) SWNTs, with diameters less than 1 nm, the photoluminescence (PL) intensities gradually decreased with the increase in the ratios of the F5 unit, followed by an abrupt decrease in PL intensity at F5 content of over 60%. Molecular mechanics simulation partially explained this behavior based on the arguments of binding energies and close packing.<sup>38</sup>



33

**Figure I-20.** Chemical structures of copolymer of 9,9-bis(*n*-decyloxy)fluorene (F10) and 9,9-bis[(*S*)-(+)-2-methylbutyl]fluorene (F5) 33.

### *1.2.5 Biomolecules*

Flavin mononucleotide has been used for the selective enrichment of (8,6) nanotubes (85% enrichment value) from a nanotube sample with broad diameter distribution. It was reported that the flavin mononucleotide could wrap around SWNTs in a helical manner that imparts efficient individualization and chirality selection. The cooperative hydrogen bonding between adjacent flavin moieties results in the formation of a helical ribbon, which organizes the dispersants around SWNTs through concentric  $\pi$ - $\pi$  interactions between the flavin mononucleotide and the underlying graphene wall. The strength of the helical flavin mononucleotide assembly is strongly dependent on nanotube chirality. In the presence of a surfactant, the flavin mononucleotide assembly is not disrupted and replaced with addition of surfactant micelles. The reason why (8, 6) SWNTs show a large affinity for the flavin mononucleotide helix has not yet been clarified.<sup>39</sup>

DNA is a naturally occurring polymer that plays a central role in biology. Single-stranded DNA also has been used to disperse SWNTs in aqueous solution. Optical absorption and fluorescence spectroscopy and AFM measurements provide evidence for individually dispersed CNTs. Molecular modelling suggests that single-stranded DNA can bind to CNTs through  $\pi$ -stacking, resulting in helical wrapping around the surface of nanotubes. The binding free energy of single-stranded DNA to CNTs rivals that of the intertube attraction. Furthermore, DNA is very efficient in dispersing SWNTs; 1 mg of DNA can disperse an equal amount of as-produced HiPCO SWNTs in 1 mL volume, yielding 0.2 to 0.4 mg mL<sup>-1</sup> CNT solution after removal of insoluble material by centrifugation.<sup>40</sup> In

addition, Dieckmann *et al.* reported that amphiphilic  $\alpha$ -helical peptides can disperse the nanotubes in an aqueous medium through peptide-peptide interactions between adjacent peptide-wrapped nanotubes to form nanofibers. The size and morphology of the fibers can be controlled by changing solution conditions that affect peptide-peptide interactions.<sup>41</sup>

### **1.3 A Brief Introduction to Tetrathiafulvalene Vinylogues (TTFVs)**

Over the past three years, diphenyl-substituted TTF vinylogues (TTFVs) have attracted our attention as appealing molecular building blocks for various functional materials, owing to their versatile redox and structural switchability and tunability. Diphenyl-substituted TTFV analogues are good electron donors, and can reversibly undergo significant conformational switching upon oxidation and reduction. In the ground state, diphenyl-TTFVs usually adopt a highly twisted molecular structure, with the two dithiole groups presenting a pseudo-cisoid conformation as a result of the steric hindrance of the two phenyl substituents and sulfur-sulfur attraction. Upon oxidation, diphenyl-TTFV undergoes a simultaneous two-electron transfer to form a stable dication. The strong electrostatic repulsion between the two dithiolium rings forces the molecules to rotate into a trans conformation, wherein the dithiolium rings are coplanar and the two phenyl moieties are nearly orthogonal to the plane of the two dithiolium rings. Figure 1-21 illustrates the bi-state conformational switching properties of a simple diphenyl-TTFV based on density functional theory (DFT) calculations.<sup>42</sup> The calculated molecular

geometry of diphenyl-TTFV and [diphenyl-TTFV]<sup>2+</sup> are in good agreement with the X-ray crystallographic data of other diphenyl-substituted TTFV derivatives.

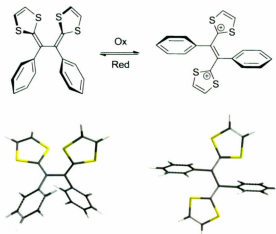
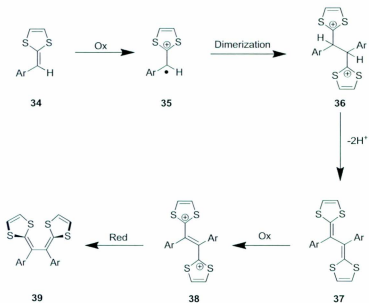


**Figure 1-21.** Redox controlled conformation switching behavior of diphenyl-TTFV.

The synthesis of TTFV requires both C–C and C=C bond formation. The most commonly used synthetic route is via the oxidative dimerization of corresponding dithiafulvene (DTF) precursors. The reaction mechanism of this dimerization was elucidated by Lorey, Hapiot, and co-workers<sup>43</sup>, and the detailed reaction steps are shown in Scheme 1-6. The first step is the oxidation of DTF **34** to generate a radical cation **35**, which then dimerizes to form a protonated dicationic TTFV **36**. The dimerized product then undergoes deprotonation to form neutral TTFV **37**. Under oxidative conditions, the neutral TTFV is

quickly converted into stable TTFV dication **38**. Finally a reduction reaction is implemented to reduce TTFV dication into neutral TTFV.<sup>42</sup>



**Scheme 1-6.** Mechanism for oxidative dimerization of aryl-DTF to form diaryl-TTFV.

#### 1.4 Outline of this thesis

This dissertation focuses on the development of noncovalent functionalization of SWNTs using redox-switchable polymer dispersants. The major objective is to devise an easily controllable and scalable approach for dispersion and release of SWNTs in solutions. It is also expected that, with rational design, the switchable dispersants may also display selectivity for particular types of SWNTs, which will eventually lead to an efficient non-

destructive and recyclable method for SWNT purification. The knowledge established by the Zhao group on TTFV chemistry shows that TTFV are an ideal redox-switching unit to make highly desirable functional polymer dispersants for SWNTs. In this light, a new class of TTFV embedded conjugated polymers was designed for investigation. This thesis outlines the progress in this topic of research. The detailed content can be divided into two parts: (1) the synthesis and properties of TTFV-phenylacetylene polymers, and (2) the side-chain effect on the TTFV polymers.

Chapter 2 describes the synthetic route to a TTFV polymer, and the properties of the TTFV polymer and its supramolecular complexes with SWNTs were studied by UV-Vis-NIR, Raman spectroscopy, atomic force microscopy (AFM), scanning electron microscopy (SEM), cyclic voltammetry, and spectroelectrochemistry. The results conclude that the TTFV polymer can reversibly disperse and release SWNTs in organic solvents under pH or redox stimuli control. Furthermore, an interesting sol-gel material composed of SWNTs-TTFV polymer was unexpectedly observed. The properties of this “bucky” gel were examined by SEM, electrochemical, and thermal analyses.

Chapter 3 describes the synthesis route to two TTFV polymer derivatives analogous to the one investigated in Chapter 2. The properties of TTFV polymer derivatives with various side chains and TTFV polymer derivatives-SWNT complexes were studied by UV-Vis-NIR, Raman spectroscopy, AFM, SEM, and cyclic voltammetry to probe the different interactions between TTFV polymer and its derivatives with SWNTs. The

results here reveal the structure-selectivity relationship for the interactions between TTFV-polymers and SWNTs.

In Chapter 4, a summary and conclusions for this MSc work are given, while perspectives are offered to point out a number of new directions worthy of pursuit in the near future.

## Chapter 2

# Synthesis and characterization of TTFV polymers and TTFV polymer–SWNTs complexes

### 2.1 Objectives of this project

SWNTs have attracted enormous interest owing to their wide spectrum of applications in materials science.<sup>44</sup> However, pristine SWNTs, as described in the previous chapter, show a strong propensity for bundling and aggregation due to significant intertube attraction; as a result, SWNTs exhibit very low solubility in various solvents, which in turn makes the direct application and processing of SWNTs problematic. To overcome this barrier, various chemical functionalization methods can be used, among which noncovalent functionalization presents a particularly intriguing approach because it can not only improve the solubility of SWNTs in a non-destructive way, but allows specific types of SWNTs to be selectively dispersed in solvents to attain enrichment or purification.<sup>45</sup> Moreover, the supramolecular complexes between SWNTs and functional macromolecular dispersants such as synthetic polymers may lead to composite materials with novel properties beneficial for the fabrication of molecular devices and nanomaterials.<sup>46</sup>

To effect SWNTs dispersion, sufficient noncovalent attractions between dispersants and SWNTs are prerequisite. Nevertheless, many dispersants show irreversible interactions with SWNTs. As a result, the reverse process to remove dispersants from SWNTs is usually not easy; in other words, how to reversibly release pristine SWNTs out of polymer matrices presents a big challenge. To address this issue, TTFV-based polymers have been designed and synthesized to reversibly disperse and release SWNTs in organic solution under the control of clean and scalable inputs such as pH or redox stimuli.

## 2.2 Introduction to molecular design

In our recent studies, a tetrathiafulvalene vinylogue (TTFV) was found to serve as a versatile molecular switching unit to exert easy conformational control at the molecular level. Phenyl-substituted TTFVs have been well known to adopt a V-shape conformation and undergo simultaneous two-electron transfer upon oxidation, which leads to dramatic *cis*-to-*trans* structural change as shown in Figure 2-1a. In the neutral state, the TTFV is twisted as result of steric hindrance while upon oxidation, the TTFV switches to a *trans* conformation due to the Coulombic repulsion between the two cationic dithiolium rings. In addition to redox conditions, our recent studies have also demonstrated that diphenyl-TTFV can be reversibly protonated to switch its conformation as shown in Figure 2-1b. These switching behaviors thus led us to the design of new types of redox and pH responsive TTFV polymers to perform reversible SWNT dispersion and release in a controlled manner as illustrated in Figure 2-1c.<sup>47,48</sup>

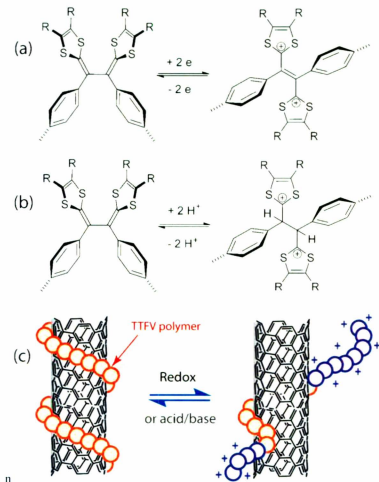


**Figure 2-1.** Bistable conformational changes of TTFV under (a) redox and (b) acid/base conditions. (c) Reversible wrapping and unwrapping of SWNT by a TTFV polymer.

In addition, molecular modelling using the molecular mechanics (MM) theory has revealed that the hexamer of TTFV phenylacetylene prefers a folded conformation in the

neutral state with a hollow inner cavity suitable for encapsulation of guests with diameters of 1–2 nm, such as an individual strand of SWNTs. As such, it was predicted that TTFV polymer in the neutral state would spontaneously form foldamers to wrap around SWNTs via favourable  $\pi$ - $\pi$  interactions, while upon oxidation or protonation the *cis*-TTFV units in the polymer would be switched to *trans*-[TTFV]<sup>2+</sup> to unfold the polymer and dissociate it from the backbone of SWNTs. Figure 2-2 shows the chemical structure of the target TTFV polymer.

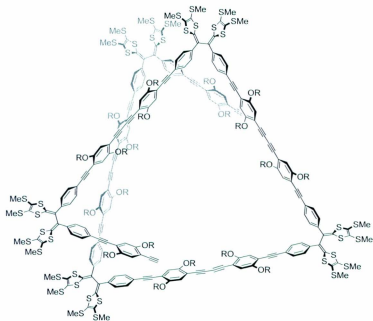


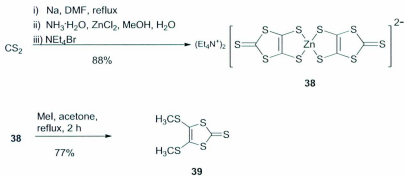
**Figure 2-2.** Structure of the designed folding TTFV polymer.

## 2.3 Results and discussion

### 2.3.1 Synthesis of TTFV polymers

#### 2.3.1.1 Synthesis of *S*-methyl thione **39**

At first, *S*-methyl thione **39** was prepared using a well-established procedure by our group. As shown in Scheme 2-1, the synthesis of *S*-methyl thione **39** started with a reaction between Na and CS<sub>2</sub> using dimethyl formamide (DMF) as solvent, and then upon addition of ZnCl<sub>2</sub> and NH<sub>3</sub>·H<sub>2</sub>O the resulting dithiolate was chelated with Zn<sup>2+</sup> and precipitated out as a stable red salt **38** in the presence of tetraethylammonium bromide. The overall yield of this sequence of reactions was 88%. Salt **38** was dissociated into free dithiolate in refluxing acetone, and the resulting intermediate was then alkylated with MeI to afford *S*-methyl thione **39** in 77% yield.

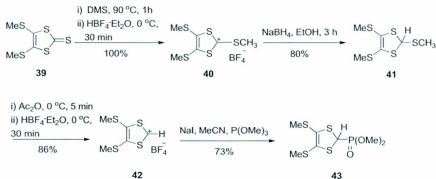


Scheme 2-1. Synthesis of *S*-methyl thione **39**.

### 2.3.1.2 Synthesis of *S*-methyl phosphonate **43**

Phosphonate **43** was synthesized based on the known procedure as shown in Scheme 2-2. *S*-methyl thione **39** first underwent alkylation with dimethyl sulfate at 100 °C. The resulting product was treated with  $\text{HBF}_4 \cdot \text{Et}_2\text{O}$  at 0 °C and precipitated out as a brown salt **40** upon addition of diethyl ether. Since the salt was not stable in air, it was immediately subjected to reduction reaction with  $\text{NaBH}_4$  in EtOH to afford **41** as a brown solid.

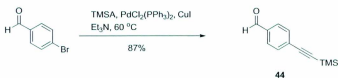
$\text{Ac}_2\text{O}$  and  $\text{HBF}_4 \cdot \text{Et}_2\text{O}$  were then added to salt **41** to afford salt **42**. The product **42** was not stable either and was immediately treated with  $\text{P}(\text{OMe})_3$  in the presence of NaI in MeCN to afford phosphonate **43** in 73% yield.



**Scheme 2-2.** Synthesis of *S*-methyl phosphonate **43**.

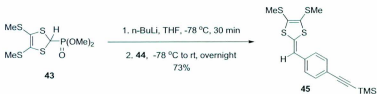
### 2.3.1.3 Synthesis of tetrathiafulvene vinylogues (TTFV) 46

The synthetic route to precursor **44** is shown in Scheme 2-3, which was developed by a group member, Dr. Guang Chen, of the Zhao group. The synthesis began with a Sonogashira reaction of 4-bromobenzaldehyde with trimethylsilylacetylene (TMSA) using  $\text{PdCl}_2(\text{PPh}_3)_2/\text{CuI}$  as catalyst in  $\text{Et}_3\text{N}$  to obtain aldehyde **44** in 87% yield.



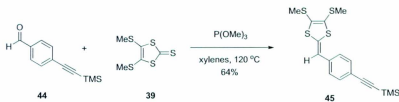
**Scheme 2-3.** Synthesis of aldehyde **44**.

Aldehyde **44** was subjected to an Horner-Wadsworth-Emmons (HWE) reaction with phosphonate **43** to produce dithiafulvene alkyne **45** in 73% yield as a yellow liquid, which solidified upon storage in the fridge.



**Scheme 2-4.** Synthesis of dithiafulvene alkyne **45**.

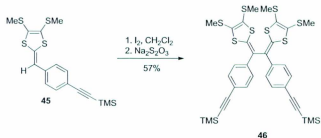
Since multiple steps are required to achieve *S*-methyl phosphonate from *S*-methyl thione **39**, the overall yield of these multiple steps is relatively low. Moreover, the use of an expensive reagent,  $\text{HBF}_4 \cdot \text{Et}_2\text{O}$ , makes the HWE strategy unsuitable for large-scale production. To circumvent this problem, a phosphite-mediated coupling strategy, which was also developed by Dr. Guang Chen in our group, was investigated as depicted in Scheme 2-5. In the presence of trimethyl phosphite, 1 molar equivalent of *S*-methyl thione **39** reacted with 1 molar equivalent of aldehyde **44** to achieve dithiafulvene alkyne **45** in xylene. Although the purification step is very tedious due to the presence of a large amount of trimethyl phosphite, dithiafulvene alkyne **45** was successfully produced by this reaction in an acceptable yield. Among different conditions tried, the solvent-free condition was found to afford the highest yield. However, in this case, much more trimethyl phosphite was needed.



**Scheme 2-5.** Alternative synthetic route to dithiafulvene alkyne **45**.

Dithiafulvene alkyne **45** was subjected to an iodine-promoted oxidative dimerization reaction as depicted in Scheme 2-6, yielding cationic dimerized products which were

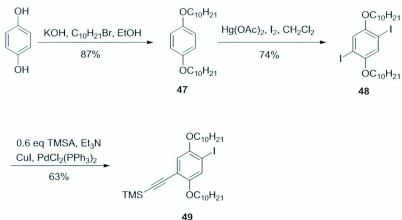
subsequently treated with  $\text{Na}_2\text{S}_2\text{O}_3$  to produce neutral phenylacetylene-substituted TTFVs **46**.



**Scheme 2-6.** Synthesis of phenylacetylene-substituted TTFVs **46**.

#### 2.3.1.4 Synthesis of aryl iodide **49**

Compound **49** was obtained by alkylation of 1,4-hydroquinone followed by iodination catalyzed by  $\text{Hg}(\text{OAc})_2$  in dichloromethane (Scheme 2-7). In the first step, commercially available 1,4-hydroquinone was subjected to an alkylation reaction with 1-bromodecane in a basic ethanolic solution to afford compound **47**. Next, compound **47** was reacted with iodine chips under the catalysis of  $\text{Hg}(\text{OAc})_2$  to produce compound **48** in a moderate yield of 65%. Finally, compound **49** underwent a Sonogashira reaction with 0.6 molar equivalent of TMSA in the presence of  $\text{Et}_3\text{N}$  and  $\text{PdCl}_2(\text{PPh}_3)_2/\text{CuI}$  catalyst to afford aryl iodide **49** in 63% yield.

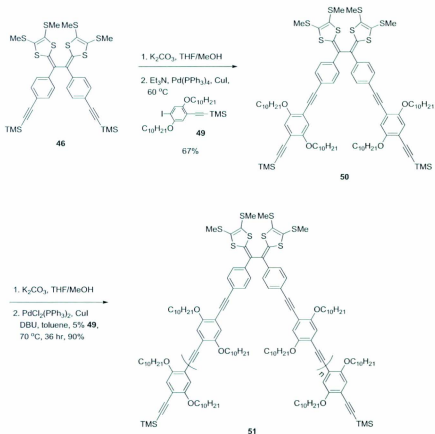


**Scheme 2-7.** Synthesis of aryl iodide **49**.

### 2.3.1.5 Synthesis of monomer **50** and TTFV polymer **51**

Phenylacetylene-substituted TTFV precursor **46** was desilylated by  $\text{K}_2\text{CO}_3$  and then cross-coupled with aryl iodide **49** in the presence of  $\text{Pd}(\text{PPh}_3)_4/\text{CuI}$  catalyst to yield monomer **50** in 67% yield as shown in Scheme 2-8. Monomer **50** was first subjected to desilylation with  $\text{K}_2\text{CO}_3$  to afford free terminal dialkyne, which then underwent a  $\text{PdCl}_2(\text{PPh}_3)_2/\text{CuI}$  catalyzed homocoupling reaction using DBU as the base in toluene, giving polymer **51**. In this polymerization, a small amount (5% mol equiv) of aryl iodide **49** was added to act as endcapping agent. The incorporation of endcapping groups in the polymer not only increased the stability of the polymer, but exerted a better control over the molecular weight and polydispersity of the polymer products. When the polymerization reaction was complete as checked by TLC analysis, crude polymer

products were precipitated out of the solution by addition of MeOH. Polymer **51** was collected as a yellow-orange solid after vacuum filtration and solvent rinsing. The resulting polymer showed good solubility in common organic solvents.



Scheme 2-8. Synthesis of monomer **50** and TTFV polymer **51**.

### 2.3.2 Characterization of TTFV polymer **51**

The molecular structure of polymer **51** was confirmed by  $^1\text{H}$  and  $^{13}\text{C}$  NMR spectroscopy. The average molecular weight and polydispersity of **51** were characterized by gel permeation chromatography (GPC), which showed  $M_w = 51900 \text{ g mol}^{-1}$ ,  $M_n = 13400 \text{ g mol}^{-1}$ , and PDI = 3.9 (Figure 2-3). The GPC data suggests the average chain length of polymer **51** is at the stage of heptamer to octamer.  $^1\text{H}$  NMR analysis of the integration ratio between protons in the endcapping group and the repeat unit indicates an average chain length of hexamer ( $n = 6$ ). Overall, the GPC and NMR analyses are in a reasonable agreement, given that GPC tends to overestimate the molecular weights of structurally rigid polymers. Molecular modeling (Figure 2-4) of the hexamer of compound **51** was performed using the molecular mechanics method (*SYBYL* force field). The computational results revealed that the polymer prefers a folded conformation via  $\pi$ -stacking to yield an inner cavity suitable for wrapping an individual SWNT.<sup>47</sup>

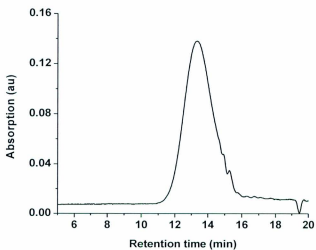


**Figure 2-3.** GPC chromatogram of TTFV polymer 51.  $M_n = 13400 \text{ g mol}^{-1}$ ,  $M_w = 51900 \text{ g mol}^{-1}$ , PDI = 3.9. Experimental conditions: columns: 2xPolyPore; standard: polystyrene; sample concentration: 1 mg polymer in 3 mL THF.

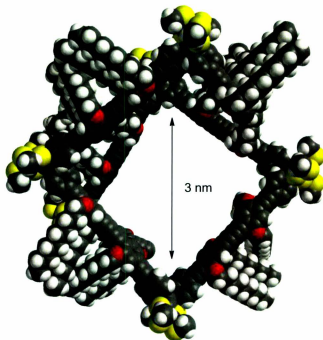


**Figure 2-4.** Optimized molecular structure of the hexamer of polymer **51** using the *SYBYL* force field implemented in Spartan<sup>10</sup>.

#### *2.3.2.1 Electronic and electrochemical properties of TTFV polymer 51.*

The electronic properties of polymer **51** and its TTFV precursors **46** and **50** were investigated by UV-Vis absorption spectroscopy. As can be seen from Figure 2-5, the maximum absorption wavelengths of compounds **46**, **50**, and **51** are observed at 381, 399, and 432 nm respectively. These absorption bands are assigned to HOMO to LUMO

electronic transitions, and the trend of steady redshift from **46** to **51** is consistent with the increasing degree of conjugation in the molecular structures.

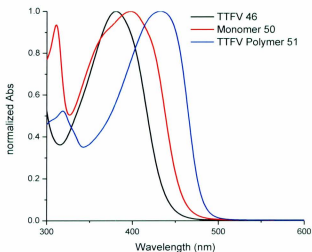


**Figure 2-5.** UV-Vis absorption spectra of compounds **46**, **50**, and **51** measured in toluene.

The electrochemical redox properties of polymer **51** and its TTFV precursors **46** and **50** were investigated by cyclic voltammetry (CV), and the detailed voltammograms are given in Figure 2-6. The CV profile of polymer **51** shows a pair of reversible redox wave pair ( $E_{pa} = +0.65$  V,  $E_{pc} = +0.52$  V) in the positive potential window. Compared to the voltammogram of TTFV **46**, the redox couple of polymer **51** can be ascribed to a simultaneous two-electron transfer at the TTFV moiety embedded in the polymer

backbone. It is also worth noting that the redox process of TTFV units in polymer **51** shows a smaller (Epa - Epc) value than that of TTFV **50**, indicating a better reversibility in electrochemical behavior. The reversible redox properties thus boded well for the expected controllable wrapping and unwrapping SWNTs as depicted in Figure 2-6.

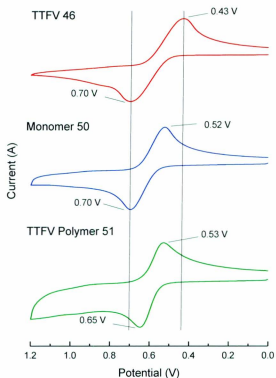


**Figure 2-6.** Cyclic voltammogram of TTFV **46**, monomer **50**, and polymer **51**. Experimental conditions: TTFV **46** ( $10^{-3}$  M), monomer **50** ( $10^{-3}$  M), and polymer **51** (2 mg/mL);  $\text{Bu}_4\text{NBF}_4$  (0.1 M) as supporting electrolyte;  $\text{CH}_2\text{Cl}_2$  as solvent; glassy carbon as

working electrode; Pt wire as counter electrode; Ag/AgCl as reference; scan rate: 200 mv/s.

#### *2.3.2.2 UV-Vis titration experiments*

The protonation behaviour of TTFV compounds **46**, **50**, and polymer **51** was investigated by UV-Vis titration with trifluoroacetic acid (TFA) in CH<sub>2</sub>Cl<sub>2</sub> at room temperature. The detailed titration data are shown in Figures 2-8 to 2-10.

The UV-Vis titration results of **46** clearly show two steps of equilibria. In the first step (Figure 2-7A), the intensity at  $\lambda = 380$  nm steadily decreases, while those at  $\lambda = 640$ , 710, and 950 nm increase. In the second step (Figure 2-7B), the intensities at  $\lambda = 640$  and 950 nm decrease, while the intensity  $\lambda = 720$  nm increases steadily. The two steps are assigned to the following protonation reactions (Figure 2-7), which lead to the formation of thiolium and dithiolium ions respectively.

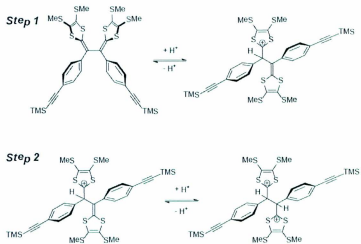


**Figure 2-7.** Protonation reactions of TTFV.

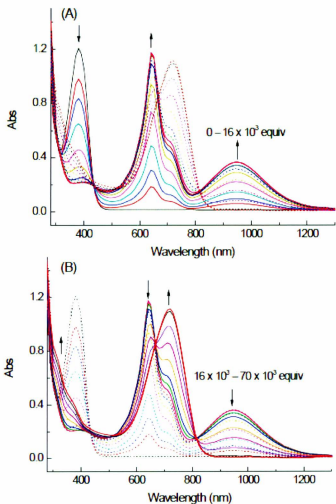


**Figure 2-8.** UV-Vis absorption spectra of TTFV 46 in  $\text{CH}_2\text{Cl}_2$  upon addition of TFA from. (A) 0 to  $1.6 \times 10^4$  equiv, and (B)  $1.6 \times 10^3$  to  $7.0 \times 10^3$  equiv. The arrows indicate the trends of spectral changes.

The titration results for monomer **50** show that the monomer **50** undergoes the same protonation processes as the TTFV precursor. In the first step (Figure 2-9A) the intensity at  $\lambda = 397\text{nm}$  steadily decreases while those at  $\lambda = 640, 710,$  and  $950\text{ nm}$  increase. In the second step (Figure 2-9B), the intensities at  $\lambda = 640$  and  $950\text{ nm}$  decrease, and the intensity  $\lambda = 720\text{ nm}$  increases steadily. For the titration results of polymer **51** (Figure 2-10), a similar protonation trend is seen as TTFV precursor, except for the trend of the intensities at  $\lambda = 415$  in the second step. When the intensities at  $\lambda = 640$  and  $950\text{ nm}$  decrease and the intensity  $\lambda = 720\text{ nm}$  increases steadily, the intensity at  $\lambda = 415$  keeps going up. The reason for this phenomenon is not clear yet, but it is believed to be associated with complex polymer conformational change.

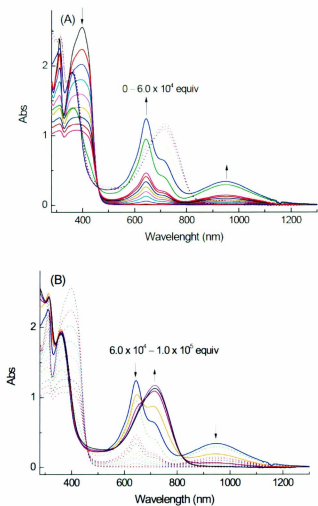


**Figure 2-9.** UV-Vis absorption spectra of monomer **50** in  $\text{CH}_2\text{Cl}_2$  upon addition of TFA from. (A) 0 to  $6.0 \times 10^4$  equiv, and (B)  $6.0 \times 10^4$  to  $1.0 \times 10^5$  equiv. The arrows indicate the trends of spectral changes.

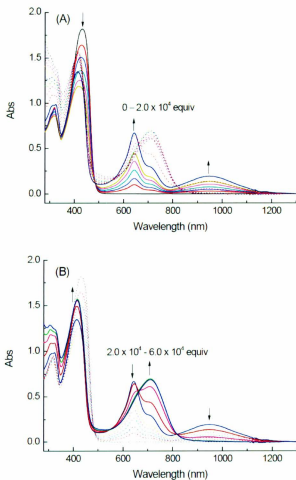


**Figure 2-10.** UV-Vis absorption spectra of polymer **51** in  $\text{CH}_2\text{Cl}_2$  upon addition of TFA from (A) 0 to  $2.0 \times 10^4$  equiv, and (B)  $2.0 \times 10^4$  to  $6.0 \times 10^4$  equiv (molar equiv was calculated based on the average molecular weight of polymer determined by GPC). The arrows indicate the trends of spectral changes.

### *2.3.2.3 AFM results of polymer 51*

AFM studies were performed on pure polymer samples, operating in the non-contact mode. Samples were prepared on freshly cleaved mica by spin coating a few drops of polymer solution onto the surface. The amount of polymer solution spin coated on the mica surface was varied, in order to get clear AFM images without big clusters. Different conditions have been investigated. Figure 2-11 shows the AFM images of the pure polymer **51**. From the top view, polymers appear as discretely distributed aggregates, and from the side view, sharp columns with the height of 4.39 nm on average are seen.

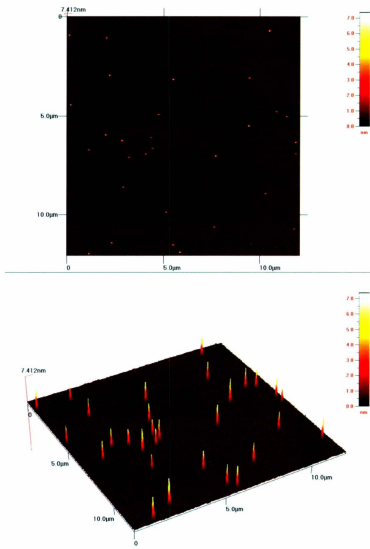


**Figure 2-11.** AFM images of pure polymer 51 spin-coated on mica.

An excess amount of TFA was added to the pure polymer solution and the acidified solution was checked with the AFM again in the non-contact mode. After acidification, polymers were discretely distributed as shown in Figure 2-12. From the side view of AFM imaging, the heights of acidified polymers were clearly increased compared with the pure ones. The average height of acidified polymers was on 8.45 nm. Conformational changes of the polymer are believed to cause the height changes. The variation of the heights of polymer aggregates on mica before and after acidification is depicted in Figure 2-13.

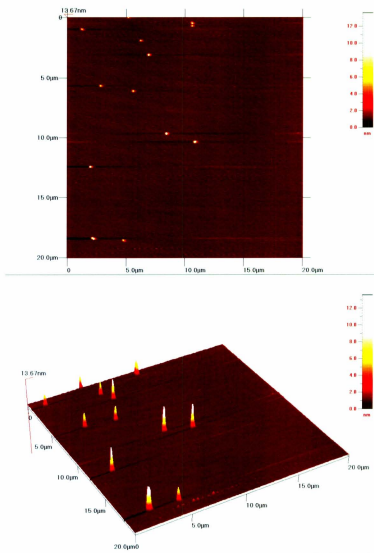


**Figure 2-12.** AFM images of acidified polymer 51 on mica.

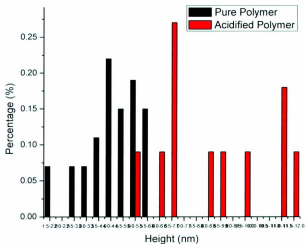


**Figure 2-13.** Statistic counts of heights of pure polymer and acidified polymer.

#### ***2.3.2.4 SEM results of polymer film and acidified polymer film***

Polymer **51** could easily form transparent and thin films upon drying under the vacuum as shown in the Figure 2-14. SEM studies were performed on a pure polymer film to investigate the morphology. Figure 2-15 shows the morphology of polymer film, where nano-discs can be observed with a diameter of 459 nm on average. Polymer units themselves could be well organized and packed together to form the observed nano-discs. Figure 2-16 shows the diameter distribution of the polymer nano-discs.

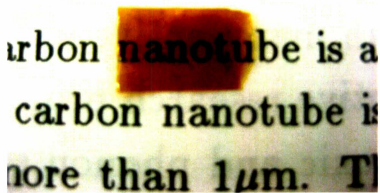
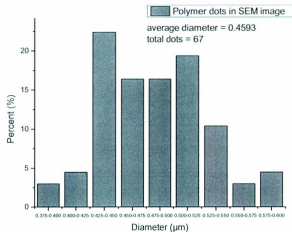


Figure2-14. Photograph of a thin film of polymer 51.



**Figure 2-15.** SEM image of polymer film 51.



**Figure 2-16.** Statistic count of diameter distribution of nano-discs on polymer film 51.

Upon exposure of the polymer film to a diluted TFA solution, the film immediately turned from yellow to green as shown in Figure 2-17. Moreover, after being immersed in aqueous  $\text{NaHCO}_3$  solution for a while, the green film could be reverted back to yellow again. Thus, this process suggests the reversible change in polymers' conformation under the control of pH input. In addition, Figure 2-18 shows the morphology of the acidified polymer film, where nano-discs disappeared and a flat and even surface was observed.

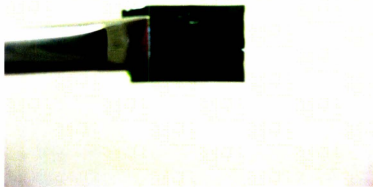


**Figure 2-17.** Photograph of acidified polymer film **51**.

### 2.3.3 Characterization of TTFV polymer–SWNTs complexes

#### 2.3.3.1 UV-Vis-NIR results of TTFV polymer–SWNTs complexes

With the polymer **51** in hand, dispersion experiments of SWNTs were then conducted, in which two commercially available SWNTs, HiPCO and CoMoCAT nanotubes, were chosen to be tested. In our experiments, pristine SWNTs were first added to the toluene solution of **51** and the mixture was subjected to ultrasonication for 30 min. After sonication, the resulting black suspension was filtered through a tightly packed cotton plug to remove insoluble components and afford a stable solution of SWNT-polymer complexes.

The SWNT-polymer complexes were then examined by UV-Vis-NIR absorption analysis, and Figure 2-19 shows the Vis-NIR absorption spectra of HiPCO and CoMoCAT nanotubes complexed with polymer **51** in toluene, which clearly give distinctive absorption bands characteristic of the electronic transitions between van Hove singularities in the electronic density of states of SWNTs. In the spectrum of CoMoCAT SWNT solution, a prominent peak at 999 nm is observed, which is assigned to SWNTs with a chiral index of (6,5). In addition, peaks at 576 and 668 nm can be assigned to (6,5) and (7,6) SWNTs respectively.<sup>29,49,50</sup> In the spectrum of HiPCO SWNT solution, the peaks appearing in the range of 930–1500 nm are attributed to inter-band transitions of semiconducting SWNTs ( $S_{11}$ ), while the peaks from 500–930 nm are due to metallic ( $M_{11}$ ) and semiconducting ( $S_{22}$ ) bands.<sup>51,52</sup> The results indicate that the SWNTs were well dispersed and debundled in the solution of polymer **51**.

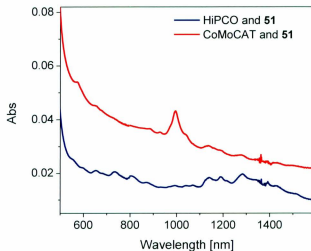


**Figure 2-19.** UV-Vis-NIR spectra of SWNTs dispersed in toluene solution of polymer **51**.

### 2.2.3.2 Raman spectroscopic results of TTFV polymer-SWNTs complexes

Evaporation of the SWNT-polymer solutions gave SWNT-polymer supramolecular complexes, which were characterized by Raman spectroscopy. Figure 2-19 shows the Raman spectra in the radial breathing mode (RBM) region. The frequencies of the Raman scattering ( $\omega_{\text{RBM}}$ ) in this region cast light on the size distributions of SWNTs dispersed by polymer **51** in toluene, since they are inversely proportional to the diameters of SWNTs ( $d_t$ ). Following the equation<sup>53</sup>,  $\omega_{\text{RBM}} = 223.5/d_t + 12.5$ , the Raman peaks in the region of 240–270  $\text{cm}^{-1}$  can be ascribed to small-diameter SWNTs ( $d_t \approx 0.8\text{--}0.9$  nm), while the

peaks at 190–210  $\text{cm}^{-1}$  are assigned to relatively large-diameter tubes ( $d_t \approx 1.2$  nm). From Figure 2-20, it can be clearly seen that the CoMoCAT SWNTs dispersed by polymer **51** are mainly composed of small-diameter tubes, while the dispersed HiPCO SWNTs contain both small and large-diameter components.<sup>54</sup>

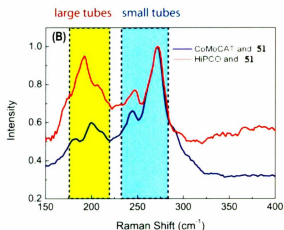


**Figure 2-20.** The RBM region of Raman spectra ( $\lambda_{\text{ex}} = 534$  nm) for SWNTs dispersed by polymer **51**.

### 2.3.3.3 AFM results of CoMoCAT SWNTs-TTFV polymer complexes

Dilute SWNT–polymer suspensions were spin-cast on a freshly cleaved mica surface to be examined by AFM imaging. Figure 2-21 depicts the AFM image of the supramolecular assemblies of CoMoCAT SWNTs and polymer **51** wherein the feature of polymer **51** wrapped around an individual strand of SWNT can be clearly observed. AFM imaging of

the assemblies of HiPCO SWNTs and polymer **51**, however, did not reveal any discrete nanotube features despite numerous trials under various conditions. Based on the Raman and AFM data, it is proposed that the interactions between folding polymer **51** and CoMoCAT tubes are predominately via the wrapping mode as depicted in Figure 2-19. For HiPCO SWNTs, it is likely that the polymer, besides wrapping around small-diameter tubes, also shows strong adhesion to the side-walls of large-diameter tubes via  $\pi$ -stacking. Such an adhesion-type binding mode could hence induce a significant degree of intertube stacking, making individual SWNT features unobservable by AFM.

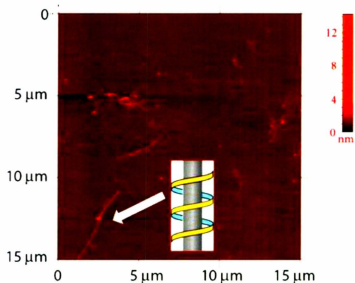


**Figure 2-21.** AFM image (tapping mode) of CoMoCAT SWNTs and polymer **51** on a mica surface.

#### *2.3.3.4 SEM images and thermogravimetric analysis (TGA) of HiPCO SWNTs-TTFV polymer gel*

The polymer-induced HiPCO SWNT stacking is also evident by the observation of gelation when the amounts of SWNTs and polymer **51** were increased to certain levels. As shown in Figure 2-22, a stable sol-gel was formed after ultrasonication of the mixture of HiPCO SWNTs and polymer **51** in toluene for 30 min. Figure 2-22 depicts the process of bulky sol-gel formation upon dispersion of 5 mg of HiPCO nanotubes in a toluene solution of polymer **51** (5 mg/mL). Table 2-1 summarizes the various conditions which have been tested for HiPCO-polymer gelation. The results give the gelation conditions, which require HiPCO nanotubes and polymer **51** to be mixed in a 1:1 mass ratio and the amount of each is higher than 5 mg/mL in toluene. SEM imaging of the resulting sol-gel showed that it is made of coarse interwoven micro-fibres (Figure 2-23). Dispersion of the gel by toluene revealed individual strands of the micro-ribbons, the widths of which are on the scale of tens of microns (Figure 2-23). In contrast, CoMoCAT SWNTs did not give rise to any gelation result when treated under the same conditions as HiPCO tubes. These results substantiate the hypothesis that the large-diameter tubes in HiPCO SWNTs interact with polymers via the surface adhesion mode to result in significant stacking, whereas CoMoCAT SWNTs containing mainly small-diameter tubes were dispersed by folding polymer **51** preferentially via wrapping. It is worth noting that polymer **51** itself does not show any gelation properties. Gelation of SWNTs with non-gelator dispersants has been rarely known,<sup>55</sup> while in our case the interactions between polymer **51** and large-diameter tubes are believed to be the key contributor to gelation.

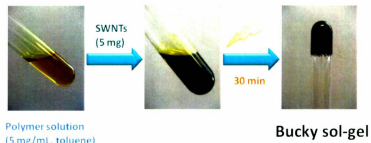


**Figure 2-22.** Photographic images illustrating the bulky sol-gel formation resulting from ultrasonication of HiPCO nanotubes and polymers **51** in toluene.

**TABLE 2-1.** Conditions that lead to the formation of HiPCO nanotube-TTFV polymer sol-gels in 1 mL of toluene.

Mass of polymer	Mass of HiPCO SWNTs	Status
1 mg	5 mg	Solution
2 mg	5 mg	Solution
3 mg	5 mg	Semi-gel
4 mg	5 mg	Semi-gel

Mass of polymer	Weight of HiPCO SWNTs	Status
5 mg	1 mg	Solution
5 mg	2 mg	Solution
5 mg	3 mg	Semi-gel
5 mg	4 mg	Semi-gel
5 mg	5 mg	Gel

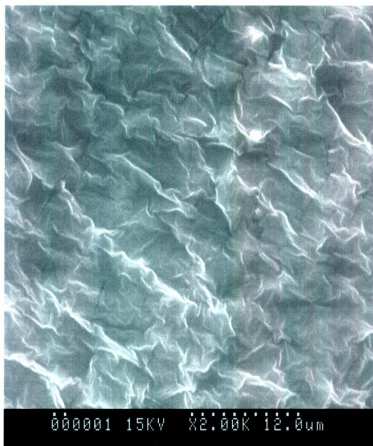


**Figure 2-23.** SEM image of the gel film of HiPCO SWNTs and polymer 51.

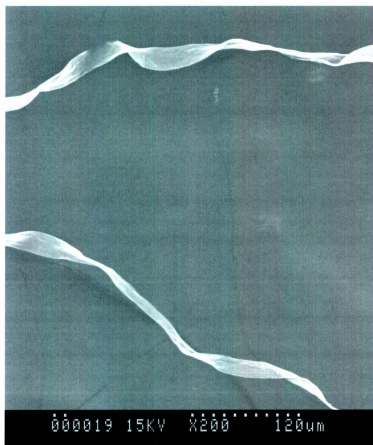


**Figure 2-24.** SEM image of diluted gel of HiPCO SWNTs and polymer 51.

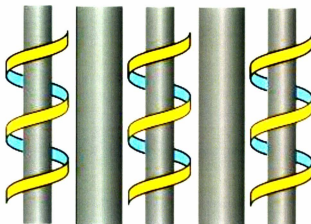


**Figure 2-25.** Schematics of polymer 51 induced stacking of HiPCO SWNTs.

Furthermore, when the sol-gel was coated evenly on the glass slide, a HiPCO SWNTs-polymer film (Figure 2-26) could be obtained after air-drying overnight. The SWNTs-polymer film was examined by CV. In this case, the SWNTs-polymer film worked as working electrode. Figure 2-27 depicts the CV profile of this SWNTs-polymer film, which indicates that the SWNTs-polymer film was conductive, although the redox peaks was not observed. In addition, the SWNTs-polymer film was also examined by TGA. Figure 2-28 shows the TGA profile of polymer film and SWNTs-polymer film, and it demonstrates that the 75% of this nanotube film is made of SWNTs, which is much higher than any of the polymer-SWNTs complexes reported so far.

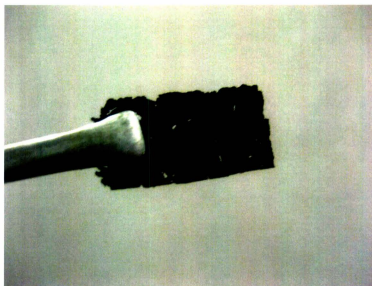


**Figure 2-26.** Photograph of HiPCO SWNTs-polymer film.

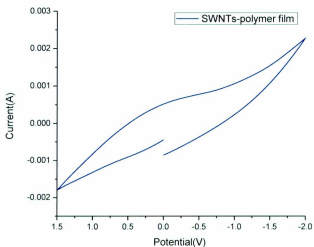


**Figure 2-27.** Cyclic voltammogram of HiPCO SWNTs-polymer xerogel. Experimental conditions:  $\text{Bu}_4\text{NBF}_4$  (0.1 M) as supporting electrolyte; acetonitrile as solvent; HiPCO SWNTs-polymer film as working electrode; Pt wire as counter electrode;  $\text{Ag}/\text{AgCl}$  as reference; scan rate: 100 mv/s.

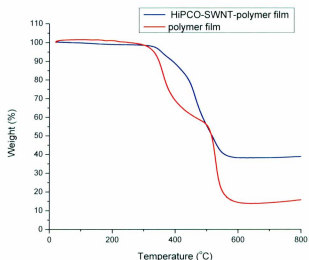


**Figure 2-28.** TGA of polymer film and HiPCO SWNTs-polymer film under  $N_2$ .

#### ***2.3.3.5 Releasing of SWNTs from TTFV polymer-SWNTs complexes and multi-cycle dispersion-releasing of SWNTs***

To dissociate polymer **51** from SWNTs, sequential chemical oxidation and reduction reactions were executed. In our experiment, iodine was chosen as the oxidant, since it can oxidize the TTFV unit of polymer **51** into  $[TTFV]^{2+}$ .<sup>48</sup> The addition of iodine to the suspension of SWNTs and polymer **51** immediately led to precipitation of SWNTs, which could be readily separated by filtration. The resulting solution of oxidized polymer **51** could be recovered by treatment with excess aq.  $Na_2S_2O_3$  to afford neutral polymer **51**, which was reusable for dispersion of SWNTs. These results validated the feasibility of

reversible dispersion and releasing of SWNTs. However, iodine oxidation was found to cause significant decomposition of polymer **51**, giving a low efficiency of polymer recovery.

To avert this problem, an alternative pH dependant approach was then attempted. Multi-cycle dispersion and releasing experiments were undertaken through the procedures described in Figure 2-29. In each cycle of dispersion, the resulting SWNT suspension was subjected to UV-Vis-NIR analysis to monitor the compositional changes in dispersed SWNTs. From Figure 2-30, it can be seen that after three cycles of dispersion/ releasing, CoMoCAT SWNTs attained noticeable enrichment of tubes with certain chirality indices. HiPCO SWNTs, on the other hand, did not show any significant compositional variation. Since polymer **51** prefers to wrap around CoMoCAT tubes, the wrapping mode is believed to give rise to chirality-selectivity to some extent. For HiPCO tubes, however, both the wrapping and the adhesion modes are at work. Hence the selectivity of polymer **51** for particular types of HiPCO SWNTs is poor.

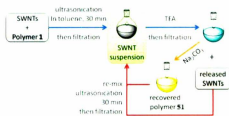


**Figure 2-29.** Schematics of multi-cycle dispersion–releasing of SWNTs in toluene solution of polymer **51**.

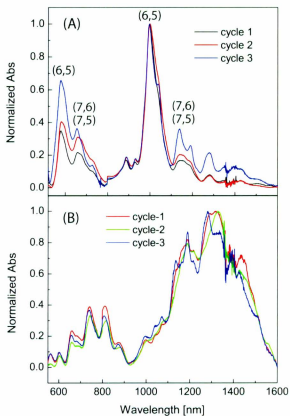


**Figure 2-30.** (A) UV-Vis-NIR absorption spectra monitoring the multi-cycle dispersion of CoMoCAT SWNTs. (B) UV-Vis-NIR absorption spectra monitoring the multi-cycle dispersion of HiPCO SWNTs.

### *2.3.3.6 Procedure of multi-cycle dispersion-releasing of CoMoCAT SWNTs*

#### Cycle 1

To a toluene solution of polymer **51** (8.0 mL, 4.5 mg/mL) was added CoMoCAT SWNTs (40 mg). The mixture was ultrasonicated for 30 min, left still for 2 h, and then filtered through a tightly packed cotton plug to remove insoluble components. A clear black SWNT solution was obtained which was characterized by UV-Vis spectral analysis.

To the solution was added an excess amount of trifluoroacetic acid (TFA, 2.0 mL). Precipitation of SWNTs was observed. The mixture was subjected to centrifugation for 15 min to afford a clear yellow solution and SWNT precipitates on the bottom. The top organic layer was carefully transferred to an Erlenmeyer flask by a pipette, washed with aq.  $\text{Na}_2\text{CO}_3$  solution, and dried over  $\text{MgSO}_4$  to afford the recovered polymer solution. UV-Vis and  $^1\text{H}$ NMR analyses on the recovered polymer showed that the recovered polymer does not undergo any changes in molecular structure. The bottom precipitates were collected and washed sequentially with toluene (20 mL) and acetonitrile (20 mL), and air-dried overnight in the fumehood to afford the released SWNTs (16 mg).

#### Cycle 2

To the released SWNTs (16 mg) was added a toluene solution of polymer **I** (3.2 mL, 4.5 mg/mL). The mixture was treated with the same procedure in cycle 1 to afford a SWNT solution, which was characterized by UV-Vis analysis.

To the solution was added an excess amount of TFA (1.0 mL). The mixture was treated with the same procedure in cycle 1 to afford the released SWNTs (3 mg) and the recovered polymer solution.

### Cycle 3

To the released SWNTs (3 mg) was added a toluene solution of polymer (0.6 mL). The mixture was treated with the same procedure in cycle 1 to afford a SWNT solution, which was characterized by UV-Vis analysis.

Then to the solution was added an excess amount of TFA (0.1 mL). The mixture was treated with the same procedure in cycle 1 to give recovered polymer solution and the released SWNTs, the weight of which was not determined due to the small amount.

**Table 2-2.** Quantities of starting and recovered CoMoCAT SWNTs, polymer solution, and TFA used in the multi-cycle dispersion-releasing of SWNTs.

	Cycle 1	Cycle 2	Cycle 3
Starting CoMoCAT NTs	40 mg	16 mg	3 mg
Polymer <b>1</b> (4.5 mg/mL)	8.0 mL	3.2 mL	0.6 mL
TFA	2.0 mL	1.0 mL	0.1 mL
Recovered CoMoCAT NTs	16 mg	3 mg*	-

\*Low recovery is presumably due to partial protonation of SWNTs and significant mechanical losses during handling of small-quantities of sample.

#### *2.2.3.7 Procedure of multi-cycle dispersion-releasing of HiPCO SWNTs*

##### Cycle 1

To a toluene solution of polymer (32.0 mL, 2.3 mg/mL) was added HiPCO SWNTs (48 mg). The mixture was ultrasonicated for 30 min, left to stand still for 2 h, and filtered through a tightly packed cotton plug to remove insoluble components. A clear black SWNT solution was obtained, which was characterized by UV-Vis spectral analysis.

To the solution was added an excess amount of TFA (3.0 mL), which led to the release of SWNTs as precipitates. The mixture was subjected to centrifugation for 15 min to afford a clear yellow solution and SWNT precipitates on the bottom. The top organic layer was carefully transferred to an Erlenmeyer flask by a pipette, washed with aq. Na<sub>2</sub>CO<sub>3</sub> solution, and dried over MgSO<sub>4</sub> to afford the recovered polymer solution. The bottom precipitates were washed sequentially with toluene (20 mL) and acetonitrile (20 mL), and air-dried overnight in the fumehood to afford the released SWNTs (10 mg).

##### Cycle 2

To the released SWNTs (10 mg) was added a toluene solution of polymer (6.0 mL, 2.3 mg/mL). The mixture was treated with the same procedure in cycle 1 to afford a SWNT solution, which was characterized by UV-Vis analysis.

To the solution was added an excess amount of TFA (0.6 mL). The mixture was treated with the same procedure in cycle 1 to afford the released SWNTs (0.5 mg) and the recovered polymer solution.

### Cycle 3

To the released SWNTs (0.5 mg) was added a toluene solution of polymer (0.3 mL, 2.3 mg/mL). The mixture was treated with the same procedure in cycle 1 to afford a SWNT solution, which was characterized by UV-Vis analysis.

To the solution was added an excess amount of TFA (0.03 mL). The mixture was treated with the same procedure in cycle 1 to give recovered polymer solution and the released SWNTs (trace).

**Table 2-3.** Quantities of starting and recovered HiPCO SWNTs, polymer solution, and TFA used in the multi-cycle dispersion-releasing of SWNTs.

	Cycle 1	Cycle 2	Cycle 3
Starting HiPCO NTs	48 mg	10 mg	0.5 mg
Polymer (2.3 mg/mL)	32 mL	6.0 mL	0.3 mL
TFA	3.0 mL	0.6 mL	0.03 mL
Recovered HiPCO NTs	10 mg	0.5 mg*	-

\*Low recovery is presumably due to partial protonation of SWNTs and significant mechanical losses during handling of small-quantities of sample.

## 2.4 Summary

The TTFV-based conjugated polymer **51** has been synthesized and it has been demonstrated that it can successfully perform reversible dispersion and release of SWNTs in a controlled manner. TTFV is an effective unit to impart the polymer with controllable, conformational switching behavior. Moreover, the supramolecular interactions between TTFV-phenylacetylene foldamer **51** and SWNTs have been demonstrated to be tube diameter-dependent. The wrapping mode facilitates the dispersion of individual small-diameter tubes, giving stable and organic soluble SWNT-polymer assemblies, while the adhesion mode works for large-diameter tubes to form supramolecular networks and produce appealing SWNT/polymer sol-gels. Finally, polymer **51** is responsive to external stimuli (redox and acidity) to allow for controllable dispersion and releasing of SWNTs in solution in a repetitive way, which opens a new avenue for developing cost-effective methods, such as continuous flow, to enrich or purify specific types of SWNTs.

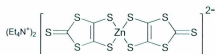
## 2.5 Experimental

Chemicals were purchased from commercial suppliers and used directly without purification. THF was distilled from sodium/benzophenone before use. Et<sub>3</sub>N and toluene were distilled from CaH<sub>2</sub> before use. Palladium catalysts, Pd(PPh<sub>3</sub>)<sub>2</sub>Cl<sub>2</sub> and Pd(PPh<sub>3</sub>)<sub>4</sub>,

were prepared from PdCl<sub>2</sub> according to literature procedures. All reactions were conducted in standard, dry glassware and under an inert atmosphere of nitrogen unless otherwise noted. Evaporation and concentration were carried out initially on a rotary evaporator and then with a vacuum pump. Flash column chromatography was performed using 240-400 mesh silica gel purchased from VWR International. Thin-layer chromatography (TLC) was carried out with silica gel 60 F254 covered on plastic sheets and visualized by UV light. <sup>1</sup>H and <sup>13</sup>C NMR spectra were measured on the Bruker Avance 500 MHz or 300 MHz spectrometers. Chemical shifts (δ) are reported in parts per million (ppm) downfield from the signal of internal reference which was SiMe<sub>4</sub>. Coupling constants (J) are given in Hertz. Infrared (IR) spectra were recorded on a Bruker Tensor 27 spectrometer equipped with a ZnSe ATR module. MALDI-TOF MS were measured on an Applied Biosystems Voyager instrument using dithranol as the matrix. UV-Vis-NIR spectra were recorded on a Cary 6000i UV-Vis-NIR spectrophotometer. Cyclic voltammetric (CV) and differential pulse voltammetric experiments were conducted in a standard three-electrode setup controlled by a BASi epsilon workstation. Trifluoroacetic acid (TFA) was used in the titration as a source of H<sup>+</sup> was purchased from Sigma Aldrich in 99% purity. HiPCO SWNTs were purchased from Carbon Nanotechnologies Inc. CoMoCAT SWNTs were purchased from Southwest NanoTechnologies Inc. The gel permeation chromatography (GPC) measurements were performed on a Waters 515 system with UV detector using polystyrene standards with THF as the eluent. Atomic force microscopy (AFM) images were taken with a Q-Scope AFM operated in tapping mode. Scanning electron microscopy (SEM) images were taken with a Hitachi S570 SEM operated

at 15 kV. Raman spectra were measured on a Horiba Jobin Yvon confocal Raman spectrometer operated at a laser wavelength of 532 nm.

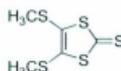
**Bis(tetraethylammonium) bis(1,3-dithiole-4,5dithiolate)zincate (38)**



**38**

Na (7.3 g, 0.320 mol) and CS<sub>2</sub> (40 mL, 0.66 mol) were mixed and the mixture was then refluxed for 20 min under N<sub>2</sub>. Dried DMF (50 mL) was added dropwise over a period of 20 min. The mixture was refluxed for 2 h and then concentrated under vacuum at 30 °C. MeOH (60 mL) was added to the residue under cooling in an ice-water bath to quench unreacted Na. A solution of ZnCl<sub>2</sub> (11.4 g, 76 mmol) in 1:1 MeOH/NH<sub>3</sub>-H<sub>2</sub>O (100 mL) was then added carefully to the filtrate. To the resulting mixture, Et<sub>4</sub>NBr (21.32 g, 102 mmol) in H<sub>2</sub>O (80 mL) was then added. Then the mixture was left standing in the fumehood overnight. The resulting mixture was then subjected to suction filtration. The residue was sequentially washed with H<sub>2</sub>O and Et<sub>2</sub>O to yield **38** as a red-colored solid (25.45 g, 35 mmol, 88%).

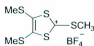
**4,5-Bis(methylthio)-1,3-dithiol-2-thione (39)**



**39**

To a solution of **38** (9.45 g, 0.013 mol) in acetone (100 mL) was added MeI (10 mL, 0.16 mol). The mixture was refluxed for overnight and filtered. The residue was washed with acetone. The filtrate was cooled in an ice bath for 0.5 h and the resulting precipitate was collected by suction filtration to afford **39** as a green crystalline solid (4.5 g, 0.020 mol, 77%). <sup>1</sup>H NMR (500 MHz, CDCl<sub>3</sub>): δ = 2.49 (s, 6H). The <sup>1</sup>H NMR data is consistent with those reported in the literature.<sup>56</sup>

#### 4,5-Bis(methylthio)-1,3-dithiol-2-ium tetrafluoroborate (**40**)

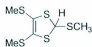


**40**

A mixture of thione **39** (4.5 g, 19.8 mmol) and DMS (15mL, 100 mmol) was heated to 100 °C and stirred for 1.5 h. The mixture was cooled under an ice bath condition, and after 5 min HBF-Et<sub>2</sub>O (5mL, 40 mmol). AcOH (12mL, 0.12 mmol) was then added. After 10 min, Et<sub>2</sub>O (120ml) was added. The precipitate was collected by filtration and washed with Et<sub>2</sub>O to afford brown solid **40** (6.2 g, 18.8 mmol, 100%). <sup>1</sup>H NMR (300 MHz,

$\text{CDCl}_3$ ):  $\delta = 3.23$  (s, 3H), 2.76 (s, 6H). The  $^1\text{H}$  NMR data is consistent with those reported in the literature.<sup>56</sup>

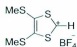
#### 4,5-Bis(methylthio)-2-(methylthio)-1,3-dithiole (**41**)



**41**

Compound **40** (6.2 mg, 18.8 mmol) was dissolved in EtOH (85 ml), and the  $\text{NaBH}_4$  (2.63 g, 69 mmol) was added under ice bath. When the mixture was warmed up to room temperature, it was stirred for 4 h. The mixture was then evaporated under vacuum.  $\text{H}_2\text{O}$  (20 ml) was added to the residue. The precipitate was collected by filtration to afford orange solid **41** (3.68g, 15 mmol, 80%).  $^1\text{H}$  NMR (300 MHz,  $\text{CDCl}_3$ ):  $\delta = 5.8$  (s, 1H), 2.42 (s, 6H), 2.27 (s, 3H). The  $^1\text{H}$  NMR data is consistent with those reported in the literature.<sup>56</sup>

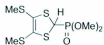
#### S-Methyl dithiolium salt (**42**)



**42**

Compound **41** (2.8 g, 12 mmol) and  $\text{Ac}_2\text{O}$  (40 ml, 0.42 mmol) were mixed under ice bath with  $\text{N}_2$ . After 5 min,  $\text{HBF}\cdot\text{Et}_2\text{O}$  (5mL, 40 mmol) was added. After 0.5 h,  $\text{Et}_2\text{O}$  (90 ml) was added. The product was collected by filtration and washed with  $\text{Et}_2\text{O}$  to produce compound **42** (2.79 g, 9 mmol, 86%) as a brown solid.  $^1\text{H}$  NMR (300 MHz,  $\text{CDCl}_3$ ):  $\delta = 11.30$  (s, 1H), 2.83 (s, 6H). The  $^1\text{H}$  NMR data is consistent with those reported in the literature.<sup>56</sup>

#### **S-Methyl phosphonate salt (43)**

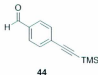


**43**

Compound **42** (1.3 g, 4 mmol) was dissolved in MeCN (30 mL). NaI (0.68g, 4.5 mmol) was then added. After 5 min,  $\text{P}(\text{OMe})_3$  (0.57mL, 4.83 mmol) was added. The mixture was stirred for 4 h. The solvent was evaporated. The residue was diluted with  $\text{CH}_2\text{Cl}_2$  and washed with  $\text{H}_2\text{O}$  till the aqueous layer became colorless. Then, the organic layer was dried over  $\text{MgSO}_4$  and evaporated to afford a dark red liquid (0.88 g, 2 mmol, 73%).  $^1\text{H}$

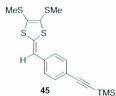
NMR (300 MHz,  $\text{CDCl}_3$ ):  $\delta = 4.72$  (d,  $J = 6.3$  Hz, 1H), 3.88 (d,  $J = 10.6$  Hz, 6H) 2.40 (s, 6H). The  $^1\text{H}$  NMR data is consistent with those reported in the literature.<sup>56</sup>

#### 4-(Trimethylsilyl ethynyl)benzaldehyde



A mixture of 4-Bromobenzaldehyde (2 g, 10.8 mmol), TMSA (3 mL, 20 mmol),  $\text{Et}_3\text{N}$  (28 mL), CuI (125 mg, 0.657 mmol) and  $\text{Pd}(\text{PPh}_3)_2\text{Cl}_2$  (150 mg, 0.213 mmol) were mixed and heated to 60 °C. The black mixture was stirred for overnight. After filtration, the filtrate was concentrated under vacuum. The residue was subjected to column chromatography (EtOAc/hexanes 1:9) to afford **44** (1.9 g, 9 mmol, 87%) as light yellow solid  $^1\text{H}$  NMR (500 MHz,  $\text{CDCl}_3$ ):  $\delta$  10.00 (s, 1H), 7.82 (d,  $J = 8.1$  Hz, 2H), 7.61 (d,  $J = 8.1$  Hz, 2H), 0.25 (s, 9H). The  $^1\text{H}$  NMR data is consistent with those reported in the literature.<sup>57</sup>

#### Acetylenic phenyldithiafulvene (45)



### Route 1

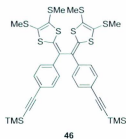
To a solution of phosphonate **43** (1.08 g, 3.35 mmol) in THF (80 ml) cooled by a dry ice bath was added *n*-BuLi (1.8 ml, 2.5 M in THF, 4.5 mmol). The mixture was stirred for 20 min and then 4-(trimethylsilyl)benzaldehyde **44** (616 mg, 3.05 mmol) in THF (20 mL) was added. The reaction mixture was allowed to be slowly warmed up to room temperature and stirred overnight. The resulting dark brown solution was diluted with Et<sub>2</sub>O, washed with H<sub>2</sub>, and dried over MgSO<sub>4</sub>. After concentration under vacuum, the residue was subjected to column chromatography (CH<sub>2</sub>Cl<sub>2</sub>/hexanes 1:9) to afford compound **45** (800 mg, 2.12 mmol, 73%) as a yellow solid <sup>1</sup>H NMR (500 MHz, CDCl<sub>3</sub>): δ 7.43 (d, *J* = 8.4 Hz, 2H), 7.13 (d, *J* = 8.3 Hz, 2H), 6.44 (s, 1H), 2.43 (d, *J* = 5.3 Hz, 6H), 0.25 (s, 9H). The <sup>1</sup>H NMR data is consistent with those reported in the literature.<sup>47</sup>

### Route 2

Bezaldehyde **39** (400 mg, 1.98 mmol), P(OMe)<sub>3</sub> (10 mL) and xylenes (20 mL) were mixed together, and the mixture was degassed and then heated to 120 °C. To the mixture was slowly added a solution of thione **39** (448 mg, 1.98 mmol) in xylenes (4 mL) over a period of 1 h. After the addition was complete, the reaction mixture was kept stirring for another 1.5 h under heating, and then it was concentrated *in vacuo*. Filtration through a

long silica plug removed the unreacted  $\text{P}(\text{OMe})_3$ . The filtrate, after concentration *in vacuo*, was subjected to silica column chromatography ( $\text{CH}_2\text{Cl}_2$ /hexanes 1:9) to yield acetylenic phenyldithiafulvene **45** (480 mg, 1.26 mmol, 64%) as a yellow solid.  $^1\text{H}$  NMR (500 MHz,  $\text{CDCl}_3$ ):  $\delta$  7.43 (d,  $J = 8.4$  Hz, 2H), 7.13 (d,  $J = 8.3$  Hz, 2H), 6.44 (s, 1H), 2.44 (s, 3H), 2.43 (s, 3H), 0.25(s, 9H). The  $^1\text{H}$  NMR data is consistent with those reported in the literature.<sup>47</sup>

#### Phenylacetylene-substituted TTFVs (**46**)



To a solution of DTF **45** (393 mg, 1.04 mmol) in  $\text{CH}_2\text{Cl}_2$  (40 mL) was added  $\text{I}_2$  (396 mg, 1.56 mmol). The resulting mixture, after being stirred for 4 h, was quenched with satd  $\text{Na}_2\text{S}_2\text{O}_3$  aq. solution (50 mL). The mixture was stirred for 2 h. Then the organic layer was separated, washed with  $\text{H}_2\text{O}$ , dried over  $\text{MgSO}_4$  and concentrated *in vacuo*. The residue was dissolved in  $\text{CS}_2$  (2 mL) and then subjected to silica column chromatography ( $\text{CH}_2\text{Cl}_2$ / hexanes 1:9) to yield phenylacetylene-substituted TTFVs **46** (224 mg, 0.295

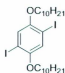
mmol, 57%) as a yellow solid.  $^1\text{H NMR}$  (500 MHz,  $\text{CDCl}_3$ ):  $\delta$  7.38 (d,  $J = 8.6\text{Hz}$ , 4H), 7.31 (d,  $J = 8.6\text{Hz}$ , 4H), 2.42 (s, 6H), 2.37(s, 6H), 0.23 (s, 18H). The  $^1\text{H NMR}$  data is consistent with those reported in the literature.<sup>47</sup>

#### 1,4-Bis(decyloxy)benzene (**47**)



Hydroquinone (4.40 g, 40 mmol), KOH (5.61 g, 99 mmol), EtOH (90 mL),  $\text{C}_{10}\text{H}_{21}\text{Br}$  (18.81 g, 90 mmol) were mixed. The resulting grey mixture was heated to  $100\text{ }^\circ\text{C}$  and refluxed for 48 h. The reaction was quenched with  $\text{H}_2\text{O}$  (100ml) and extracted with  $\text{CH}_2\text{Cl}_2$ . The organic layer was washed with  $\text{NH}_4\text{Cl}$ ,  $\text{H}_2\text{O}$ , and brine and dried over  $\text{MgSO}_4$ . The filtrate was concentrated under vacuum. The off-white solid was recrystallized from MeOH. The resulting colorless flakes were washed with cold MeOH to produce **47** as white flakes solid (13.6 g, 34 mmol, 87%).  $^1\text{H NMR}$  (300 MHz,  $\text{CDCl}_3$ ):  $\delta = 6.81$  (s, 4 H), 3.88 (t,  $J = 6.59\text{ Hz}$ , 4H), 1.77-1.72 (m, 4H), 1.46-1.27 (m, 28H), 0.89 (t,  $J = 6.45\text{ Hz}$ , 6H). The  $^1\text{H NMR}$  data is consistent with those reported in the literature.<sup>56</sup>

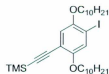
#### 1,4-Bis(decyloxy)-2,5-diiodobenzene (**48**)



**48**

**47** (5.86 g, 15 mmol), I<sub>2</sub> (9.39 g, 37 mmol), Hg(OAc)<sub>2</sub> (11.79 g, 37 mmol) and CH<sub>2</sub>Cl<sub>2</sub> (80 mL) were mixed and stirred for 24 h. Then it was filtered and washed with Na<sub>2</sub>S<sub>2</sub>O<sub>3</sub>, water, brine, and dried over MgSO<sub>4</sub>. The solvent was removed under vacuum. The crude product was recrystallized from EtOH to afford the compound **48** as white solid (7.13 g, 11 mmol, 74%). <sup>1</sup>H NMR (500 MHz, CDCl<sub>3</sub>): δ 7.17 (s, 2H), 3.94 (t, *J* = 6.44 Hz, 4H), 1.82-1.76 (m, 4H), 1.38-1.20 (m, 28H), 0.90 (t, *J* = 6.79 Hz, 6H). The <sup>1</sup>H NMR data is consistent with those reported in the literature.<sup>56</sup>

#### 1,4-Bis(decyloxy)-2-iodo-5-(trimethylsilylethynyl)benzene (**49**)

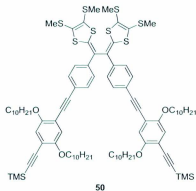


**49**

A mixture of **48** (4.23 g, 6.59 mmol), Pd(PPh<sub>3</sub>)<sub>2</sub>Cl<sub>2</sub> (0.189 g, 0.27 mmol), and CuI (0.125 g, 0.66 mmol) were added in 60 mL of Et<sub>3</sub>N. Then TMSA (0.67 mL, 4.6 mmol) was

added dropwise. The reaction mixture was then stirred at 60 °C for 24 h. The resulting mixture was filtrated and the filtrate was washed with NH<sub>4</sub>Cl, H<sub>2</sub>O, and brine and dried over MgSO<sub>4</sub>. The solvent was removed under vacuum. It was then subjected to column chromatography (hexanes/CH<sub>2</sub>Cl<sub>2</sub>, 9:1) to afford compound **49** (1.75 g, 2.8 mmol, 63%) as a colorless liquid. <sup>1</sup>H NMR (500 MHz, CDCl<sub>3</sub>): δ = 7.25 (s, 1 H), 6.83 (s, 1H), 3.95-3.92 (m, 4H), 1.82-1.75 (m, 4H), 1.52-1.46 (m, 4H), 1.34-1.27 (m, 24H), 0.88 (t, *J* = 6.57, 6H), 0.25 (s, 9H). The <sup>1</sup>H NMR data is consistent with those reported in the literature.<sup>56</sup>

#### TTFV monomer (**50**)



To a solution of TTFV **46** (83 mg, 0.11 mmol) in THF/MeOH (10 mL, 1:1) was added K<sub>2</sub>CO<sub>3</sub> (91 mg, 0.66 mmol). The mixture was stirred for 0.5 h at room temperature, and then diluted with CH<sub>2</sub>Cl<sub>2</sub>, washed with H<sub>2</sub>O, dried over MgSO<sub>4</sub>, and concentrated *in vacuo*. To the residue was added Et<sub>3</sub>N (30 mL) and iodoarene **49** (269 mg, 0.440 mmol). The mixture was degassed by vigorous N<sub>2</sub> bubbling. To the mixture was then added CuI

(12 mg, 0.011 mmol) and Pd(PPh)<sub>4</sub> (6 mg, 0.03 mmol). The mixture was heated at 60 °C and kept stirring overnight. The resulting reaction mixture was diluted with CH<sub>2</sub>Cl<sub>2</sub>, washed sequentially with aq. NH<sub>4</sub>Cl and H<sub>2</sub>O, dried over MgSO<sub>4</sub>, and concentrated *in vacuo*. The residue was purified by silica column chromatography (CH<sub>2</sub>Cl<sub>2</sub>/hexanes 5:95) to yield TTFV monomer **50** (116 mg, 0.0732 mmol, 67%) as a yellow oil. <sup>1</sup>H NMR (500 MHz, CDCl<sub>3</sub>) δ 7.45 (d, *J* = 8.5 Hz, 4H), 7.37 (d, *J* = 8.4 Hz, 4H), 6.92 (d, *J* = 5.1 Hz, 4H), 4.00–3.93 (m, 8H), 2.40 (d, *J* = 24.3 Hz, 12H), 1.84 – 1.75 (m, 8H), 1.53 – 1.46 (m, 8H), 1.39–1.19 (m, 48H), 0.86 (m, 12H), 0.25 (s, 18H); <sup>13</sup>C NMR (75 MHz, CDCl<sub>3</sub>) δ 154.18, 153.45, 137.91, 136.64, 131.87, 128.77, 126.30, 125.09, 123.64, 121.51, 117.28, 116.87, 114.31, 113.65, 101.20, 100.06, 95.01, 86.74, 69.58, 69.50, 31.91, 29.66, 29.62, 29.56, 29.46, 29.39, 29.36, 29.31, 26.06, 26.00, 22.71, 18.95, 18.86, 14.18, 14.14; FTIR (neat) 2922, 2854, 2152, 1503, 1465, 1475, 1378, 1277, 1213, 1019 cm<sup>-1</sup>; HR-MALDI-TOF MS *m/z* calcd for C<sub>90</sub>H<sub>126</sub>O<sub>4</sub>S<sub>8</sub>Si<sub>2</sub> 1582.6960, found was 1582.7006.



1.51 – 1.43 (m, 55H), 1.39 – 1.19 (m, 445H), 0.90 – 0.79 (m, 128H), 0.06 (s, 18H);  $^{13}\text{C}$  NMR (75 MHz,  $\text{CDCl}_3$ )  $\delta$  155.00, 153.47, 138.08, 137.89, 136.75, 131.93, 129.05, 128.81, 128.24, 126.32, 125.31, 125.13, 123.60, 121.41, 117.71, 116.93, 115.18, 112.53, 95.69, 86.66, 79.62, 79.35, 69.82, 69.61, 31.93, 29.73, 29.64, 29.61, 29.57, 29.49, 29.38, 29.29, 29.17, 26.06, 26.01, 25.96, 22.72, 21.48, 18.97, 18.87, 14.19, 14.14. FTIR (neat) 2915, 2849, 2202, 1509, 1467, 1417, 1376, 1272, 1211, 1017  $\text{cm}^{-1}$ . GPC:  $M_n = 13400 \text{ g mol}^{-1}$ ,  $M_w = 51900 \text{ g mol}^{-1}$ , PDI = 3.9.

## Chapter 3

# Side-Chain Effect on Dispersion of SWNTs with TTFV Polymers

### 3.1 Objective of the Project

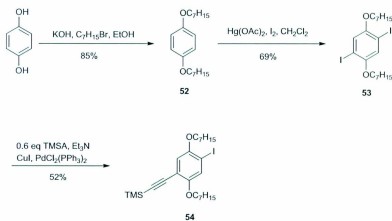
From the studies described in the previous chapter, the TTFV polymers have been known to interact with SWNTs to form soluble supramolecular assemblies. The major interaction mode is through  $\pi$ -stacking between the aromatic units of the polymer and the surface of SWNT. In addition to that, the long alkyl chains on the polymer backbone can also induce C-H/ $\pi$  interactions to facilitate the dispersion of SWNTs. The two types of interactions are supposed to both come into play significantly; however, their effects on the selectivity towards different types of SWNTs cannot be clarified from the results of previous studies. To cast light on this issue, further investigations on the side-chain effect are needed. In this chapter, two analogous TTFV polymers were chosen to be studied. The polymers have the same  $\pi$ -conjugated backbone as the TTFV polymer reported in the previous chapter but the side chains were systematically varied from *n*-pentyl to *n*-heptyl structures.

### 3.2 Result and Discussion

### 3.2.1 Synthesis of TTFV polymers 59 and 61

#### 3.2.1.1 Synthesis of aryl iodide 54

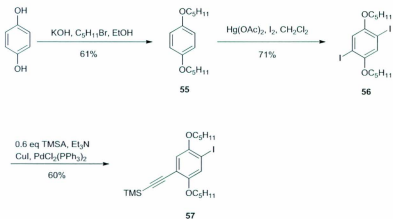
In the first step, commercially available 1,4-hydroquinone was subjected to an alkylation reaction with 1-bromoheptane in a basic ethanol solution to afford compound **52** (Scheme 3-1). Compound **52** underwent an iodination reaction in the presence of iodine chips and  $\text{Hg}(\text{OAc})_2$  to produce compound **53** in a moderate yield of 69%. Finally, compound **53** underwent a Sonogashira coupling reaction with 0.6 molar equivalent of TMSA in the presence of  $\text{Et}_3\text{N}$  and  $\text{PdCl}_2(\text{PPh}_3)_2/\text{CuI}$  catalysts to afford aryl iodide **54** in 52% yield.



Scheme 3-1. Synthesis of aryl iodide **54**.

### 3.2.1.2 Synthesis of aryl iodide 57

Commercially available 1,4-hydroquinone was subjected to an alkylation reaction with 1-bromopentane in a basic ethanol solution to afford compound **55** (Scheme 3-2). Iodination of compound **55** with iodine chips under the catalysis of  $\text{Hg}(\text{OAc})_2$  produced compound **56** in a moderate yield of 71%. Finally, compound **56** underwent a Sonogashira reaction with 0.6 molar equivalent of TMSA in the presence of  $\text{Et}_3\text{N}$  and  $\text{PdCl}_2(\text{PPh}_3)_2/\text{CuI}$  catalysts to afford aryl iodide **57** in 60% yield.

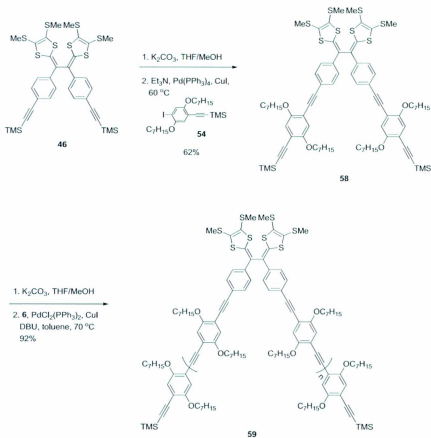


Scheme 3-2. Synthesis of aryl iodide 57.

### 3.2.1.3 Synthesis of monomer 58 and polymer 59

Phenylacetylene-substituted TTFV precursor **46** was desilylated by  $\text{K}_2\text{CO}_3$  and then cross-coupled with aryl iodide **54** in the presence of  $\text{Pd}(\text{Ph}_3)_4/\text{CuI}$  catalysts to yield

monomer **58** in 62% yield as shown in Scheme 3-3. With monomer **58** in hand, it was subjected to desilylation with  $K_2CO_3$ , and the resulting free terminal dialkyne product was subjected to a  $PdCl_2(Ph_3)_2/CuI$  catalyzed homocoupling reaction with DBU as base in toluene, giving polymer **59**. In this polymerization step, a small amount (5% mol equiv) of aryl iodide **54** was added to act as endcapping agent. The incorporation of endcapping groups in the polymer not only increases the stability of the polymer, but exerts better control over the molecular weight and polydispersity of the polymeric products. When the polymerization reaction was complete as indicated by TLC analysis, the resulting crude polymer products were precipitated out of the solution by addition of MeOH. Polymer **59** was collected as a yellow-orange solid after vacuum filtration. The resulting polymer showed good solubility in common organic solvents.

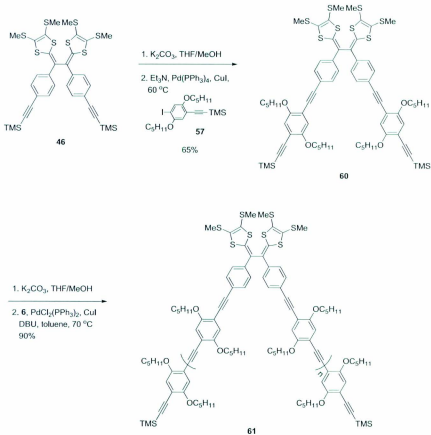


**Scheme 3-3.** Synthesis of monomer **58** and TTFV polymer **59**.

#### 3.2.1.4 Synthesis of monomer **60** and polymer **61**

Phenylacetylene-substituted TTFV precursor **46** was desilylated by  $K_2CO_3$  and then cross-coupled with aryl iodide **57** in the presence of  $Pd(PPh_3)_4/CuI$  catalysts to yield

monomer **60** in 67% yield as shown in Scheme 3-4. Monomer **60** was then desilylated with  $K_2CO_3$ , followed by a  $PdCl_2(Ph_3)_2/CuI$  catalyzed homocoupling reaction with DBU as base in toluene, giving polymer **61**. In this polymerization step, a small amount (5% mol equiv) of aryl iodide **57** was added to act as endcapping agent. When the polymerization reaction was complete as checked by TLC analysis, crude polymer products were precipitated out of the solution by addition of MeOH. Polymer **61** was collected as a yellow-orange solid after vacuum filtration, and the resulting polymer showed good solubility in common organic solvents.



**Scheme 3-4.** Synthesis of monomer **60** and TTFV polymer **61**.

### *3.2.2 Characterization of TTFV polymers 59 and 61 and their complexes with SWNTs*

#### *3.2.2.1 Electrochemical properties of polymers 59 and 61*

The electrochemical redox properties of polymers **59** and **61** were investigated by cyclic voltammetry (CV), and their cyclic voltammograms were compared with polymer **51** as shown in Figure 3-1. The CV profiles of polymers **59** and **61** show reversible redox wave pairs in the positive potential window. Compared to the voltammogram of TTFV **46**, the redox couples of polymers **59** and **61** can be ascribed to simultaneous two-electron transfer at the TTFV moieties embedded in the polymer backbone. It is also worth noting that the redox processes arising from the TTFV units in polymers **59** and **61** give a similar ( $E_{pa} - E_{pc}$ ) value to that of polymer **51**, which means that slight changes in the side-chain structures have little effect on the redox reversibility of the TTFV polymers.

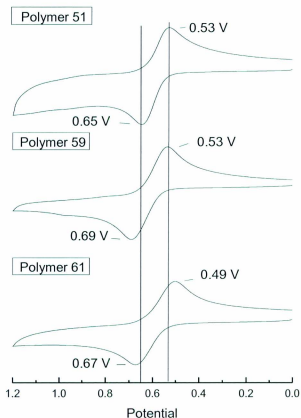


**Figure 3-1.** Cyclic voltammogram of polymer **51**, polymer **59**, and polymer **61**. Experimental conditions: polymer **51** (ca. 2 mg/mL), polymer **59** (ca. 10 mg/mL), polymer **61** (ca. 10 mg/mL);  $\text{Bu}_4\text{NBF}_4$  (0.1 M) as supporting electrolyte;  $\text{CH}_2\text{Cl}_2$  as solvent; glassy carbon as working electrode; Pt wire as counter electrode; Ag/AgCl as reference; scan rate: 200 mv/s.

### 3.2.2.2 Characterization of TTFV polymers and SWNTs complexes

#### 3.2.2.2.1 UV-Vis-NIR absorption properties

With two new TTFV polymers in hand, dispersion experiments of SWNTs were then conducted following the procedures described in the previous chapter. The resulting SWNT-polymer supramolecular complexes were examined by UV-Vis-NIR absorption analysis.

Figure 3-2 compared the normalized Vis-NIR absorption spectra of CoMoCAT nanotubes complexed with polymers **51**, **59**, and **61** in toluene. It can be clearly seen that as the side chains of the polymers became shorter, the maximum absorption band at 994 nm became narrower, indicating that better selectivity for CoMoCAT SWNTs can be achieved by using TTFV polymers carrying shorter alkyl side chains. On the other hand, no significant differences can be observed in the Vis-NIR spectral region for HiPCO SWNTs complexed with polymers **51**, **59**, and **61** (Figure 3-3).

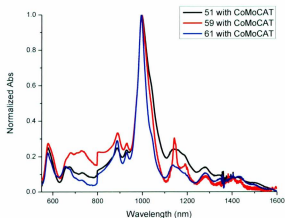


**Figure 3-2.** Normalized UV-Vis-NIR absorption spectra of CoMoCAT SWNTs with polymers **51**, **59**, and **61**.

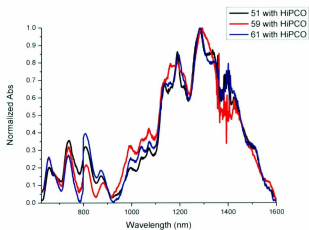


**Figure 3-3.** Normalized UV-Vis-NIR absorption spectra of HiPCO SWNTs complexed with **51**, **59**, and **61**.

### 3.2.2.2.2 Raman spectroscopic properties

TTFV polymer-SWNTs supramolecular complexes were characterized by Raman spectroscopy. Figures 3-8 and 3-9 show the Raman spectra in the radial breathing mode (RBM) region. The frequencies of the Raman scattering ( $\omega_{\text{RBM}}$ ) in this region are inversely proportional to the diameters of SWNTs ( $d_t$ ) dispersed by polymer **59** and **61** in toluene according to the following equation,  $\omega_{\text{RBM}} = 223.5/d_t + 12.5$ . For CoMoCAT SWNTs-TTFV polymer complexes, it can be clearly seen that there was no difference for small diameter tubes dispersed by the three polymers, but as the side chains of polymer became shorter, less amounts of large-diameter tubes were dispersed. This trend can be clearly seen from the spectral patterns in the region of 190–210  $\text{cm}^{-1}$ . The similar trend can be seen on HiPCO tubes dispersed by the three polymers as well. Furthermore, compared with pristine CoMoCAT SWNTs, polymer **61** shows the best performance in terms of dispersing narrowly distributed CoMoCAT SWNTs.

The dispersion results may be rationalized by assuming that, in addition to wrapping themselves around small-diameter tubes, the side chains of the polymers can also interact with the side walls of large diameter tubes via C-H/ $\pi$  interactions as shown in Figure 3-6. As the side chains of polymers became shorter, this interaction became weaker. Therefore, the amount of large tubes dispersed by the polymers decreases.

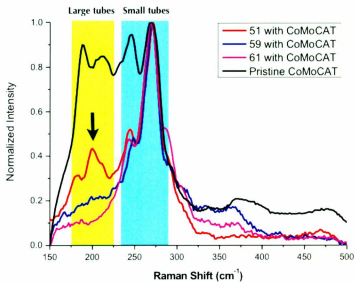


**Figure 3-4.** The RBM region of Raman spectra ( $\lambda_{\text{ex}} = 534 \text{ nm}$ ) for pristine CoMoCAT SWNTs and CoMoCAT SWNTs dispersed by polymers **51**, **59** and **61**.

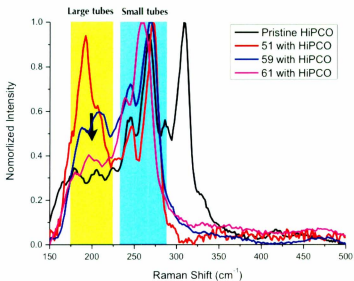


**Figure 3-5.** The RBM region of Raman spectra ( $\lambda_{\text{ex}} = 534 \text{ nm}$ ) for pristine HiPCO SWNTs and HiPCO SWNTs dispersed by polymer **51**, **59** and **61**.

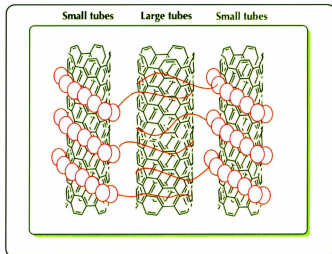


**Figure 3-6.** Schematic illustration of the effect of side chains in polymers **51**, **59** and **61** on binding to carbon nanotubes.

### 3.2.2.2.3 Results of AFM imaging

Dilute SWNT-polymer suspensions were spin-cast on a freshly cleaved mica surface for AFM imaging. Contact mode was used to get better imaging results, but discrete HiPCO SWNTs-polymer complexes were not detected in the contact mode despite numerous trials under various conditions. Figure 3-7 depicts the AFM image (contact mode) of the supramolecular assemblies of CoMoCAT SWNTs and polymer **59**, where the features of polymer **59** wrapping around individual strands of SWNTs can be observed. AFM

imaging (Figure 3-8) of the assemblies of CoMoCAT SWNTs and polymer **61** shows similar results.

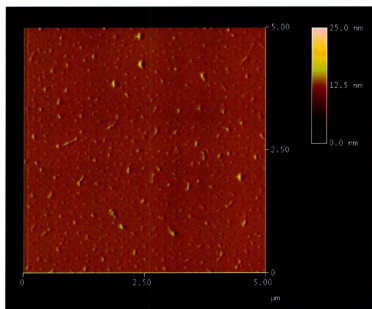


**Figure 3-7.** AFM image (contact mode) of CoMoCAT SWNTs and polymer **59** on a mica surface.

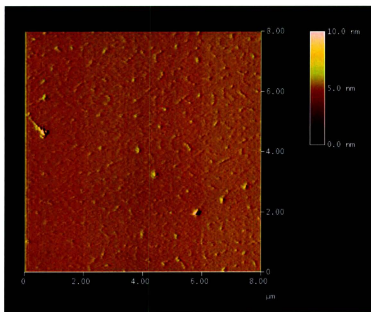


**Figure 3-8.** AFM image (contact mode) of CoMoCAT SWNTs and polymer **61** on a mica surface.

### 3.3 Summary

Two new TTFV polymers **59** and **61** have been synthesized and characterized to demonstrate that side chains changes have little effect on redox properties. Polymers **59** and **61** still retain property of reversibility controlled by redox and pH inputs. TTFV polymers **59** and **61** can effectively disperse SWNTs in organic solvents, giving stable and soluble SWNT–polymer assemblies. In addition to wrapping around SWNTs, the side chains of polymers can interact with large diameter tubes via alkyl- $\pi$  interactions. Raman

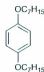
spectral analyses indicates that polymers with shorter side chains interact with SWNTs mainly by wrapping the conjugated polymer backbone around SWNTs. The wrapping mode gives rise to selectivity for small-diameter tubes. In the case of polymers containing long alkyl side chains, the alkyl- $\pi$  interaction tends to entangle large-diameter tubes in the polymer matrix. As a result, SWNTs can be better solubilized by TTFV polymers with long alkyl side chains, but the selectivity for the tube diameter is reduced.

### 3.4 Experimental

Chemicals were purchased from commercial suppliers and used directly without purification. THF was distilled from sodium/benzophenone before use. Et<sub>3</sub>N and toluene were distilled from CaH<sub>2</sub> before use. Palladium catalysts, Pd(PPh<sub>3</sub>)<sub>2</sub>Cl<sub>2</sub> and Pd(PPh<sub>3</sub>)<sub>4</sub>, were prepared from PdCl<sub>2</sub> according to literature procedures. All reactions were conducted in standard, dry glassware and under an inert atmosphere of nitrogen unless otherwise noted. Evaporation and concentration were carried out with a water-aspirator. Flash column chromatography was performed using 240–400 mesh silica gel purchased from VWR International. Thin-layer chromatography (TLC) was carried out with silica gel 60 F254 covered on plastic sheets and visualized by UV light. <sup>1</sup>H and <sup>13</sup>C NMR spectra were measured on Bruker Avance 500 MHz or 300 MHz spectrometers. Chemical shifts ( $\delta$ ) are reported in parts per million (ppm) downfield from the signal of internal reference SiMe<sub>4</sub>. Coupling constants (*J*) are given in Hertz. Infrared (IR) spectra were recorded on a Bruker Tensor 27 spectrometer equipped with a ZnSe ATR module. MALDI-TOF MS were measured on an Applied Biosystems Voyager instrument using

dithranol as the matrix. UV-Vis-NIR spectra were recorded on a Cary 6000i UV-Vis-NIR spectrophotometer. Cyclic voltammetric (CV) and differential pulse voltammetric experiments were conducted in a standard three-electrode setup controlled by a BASi epsilon workstation. Trifluoroacetic acid (TFA) was used in the titration as a source of  $H^+$  was purchased from sigma Aldrich in 99% purity. HiPCO SWNTs were purchased from Carbon Nanotechnologies Inc. CoMoCAT SWNTs were purchased from Southwest NanoTechnologies Inc. The gel permeation chromatography (GPC) measurements were performed on a Waters 515 system with UV detector using polystyrene standards with THF as eluent. Atomic force microscopy (AFM) images were taken with a MultiNode<sup>TM</sup> SPM from digital Instruments operated in contact mode. Raman spectra were measured on a Horiba Jobin Yvon confocal Raman spectrometer operated at a laser wavelength of 532nm.

#### 1,4-Bis(decyloxy)benzene (52)

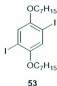


52

Hydroquinone (5.2 g, 47 mmol), KOH (10.19 g, 188 mmol), EtOH (50 mL),  $C_{10}H_{21}Br$  (32.88 g, 188 mmol) were mixed. The resulting grey mixture was heated to 90 °C and refluxed for 48 h. The reaction was quenched with  $H_2O$  (100ml) and extracted with

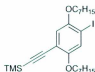
$\text{CH}_2\text{Cl}_2$ . The organic layer was washed with  $\text{NH}_4\text{Cl}$ ,  $\text{H}_2\text{O}$ , and brine and dried over  $\text{MgSO}_4$ . The filtrate was concentrated under vacuum. The off-white solid was recrystallized from MeOH. The resulting colorless flakes were washed with cold MeOH to produce **52** as a white, flaky solid (11.73 g, 38 mmol, 85%).  $^1\text{H}$  NMR (300 MHz,  $\text{CDCl}_3$ ):  $\delta$  6.82 (s, 4H), 3.90 (t,  $J = 6.44$  Hz, 4H), 1.80-1.70 (m, 4H), 1.48-1.30 (m, 16H), 1.36-1.32 (m, 24H), 0.89 (t,  $J = 6.79$  Hz, 6H). The  $^1\text{H}$  NMR data is consistent with those reported in the literature.<sup>58</sup>

#### 1,4-Bis(decyloxy)-2,5-diiodobenzene (**53**)



**52** (5.86 g, 17 mmol),  $\text{I}_2$  (12.95 g, 51 mmol),  $\text{Hg}(\text{OAc})_2$  (16.25 g, 51 mmol) and  $\text{CH}_2\text{Cl}_2$  (50 mL) were mixed and stirred for 24 h. Then the reaction mixture was filtered and washed with  $\text{Na}_2\text{S}_2\text{O}_3$ , water, brine, and dried over  $\text{MgSO}_4$ . The solvent was removed under vacuum. The crude product was recrystallized from EtOH to afford the compound **53** as white solid (6.6 g, 11 mmol, 69%).  $^1\text{H}$  NMR (500 MHz,  $\text{CDCl}_3$ ):  $\delta$  7.17 (s, 2H), 3.92 (t,  $J = 6.44$  Hz, 4H), 1.82-1.77 (m, 4H), 1.52-1.46 (m, 4H), 1.39-1.32 (m, 12H), 0.90 (t,  $J = 6.79$  Hz, 6H). The  $^1\text{H}$  NMR data is consistent with those reported in the literature.<sup>59</sup>

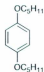
**1,4-Bis(decyloxy)-2-iodo-5-(trimethylsilylethynyl)benzene (54)**



**54**

A mixture of **53** (10 g, 17.8 mmol), Pd(PPh<sub>3</sub>)<sub>2</sub>Cl<sub>2</sub> (0.24 g, 0.36 mmol), and CuI (0.2 g, 1.1 mmol) were added to 100 mL of Et<sub>3</sub>N. Then TMSA (1.83 mL, 12.46 mmol) was added dropwise. The reaction mixture was then stirred at 60 °C for 24 h. The resulting mixture was filtered and the filtrate was washed with NH<sub>4</sub>Cl, H<sub>2</sub>O, and brine and dried over MgSO<sub>4</sub>. The solvent was removed under vacuum. It was then subjected to column chromatography (hexanes/CH<sub>2</sub>Cl<sub>2</sub>, 9:1) to afford compound **54** (3.44 g, 6 mmol, 52%) as a colorless liquid. <sup>1</sup>H NMR (500 MHz, CDCl<sub>3</sub>): δ = 7.25 (s, 1 H), 6.83 (s, 1H), 3.95-3.91 (m, 4H), 1.83-1.74 (m, 4H), 1.53-1.45 (m, 4H), 1.26-1.38 (m, 16H), 0.98-0.85 (m, 12H), 0.25 (s, 9H).<sup>59</sup>

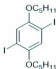
**1,4-Bis(decyloxy)benzene (55)**



55

Hydroquinone (5.0 g, 45 mmol), KOH (7.57 g, 135 mmol), EtOH (50 mL),  $C_{10}H_{21}Br$  (27.0 g, 180 mmol) were mixed. The resulting grey mixture was heated to 100 °C and refluxed for 48 h. The reaction was quenched with  $H_2O$  (100ml) and extracted with  $CH_2Cl_2$ . The organic layer was washed with  $NH_4Cl$ ,  $H_2O$ , and brine and dried over  $MgSO_4$ . The filtrate was concentrated under vacuum. The off-white solid was recrystallized from MeOH. The resulting colorless flakes were washed with cold MeOH to produce **55** as white flakes solid (6.91 g, 27 mmol, 61%).  $^1H$  NMR (300 MHz,  $CDCl_3$ ):  $\delta$  = 6.82 (s, 4 H), 3.90 (t,  $J$  = 6.59 Hz, 4H), 1.80-1.71 (m, 4H), 1.48-1.31 (m, 8H), 0.92 (t,  $J$  = 6.45 Hz, 6H). The  $^1H$  NMR data is consistent with those reported in the literature.<sup>60</sup>

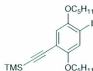
#### 1,4-Bis(decyloxy)-2,5-diiodobenzene (**56**)



56

**55** (3.17 g, 12 mmol), I<sub>2</sub> (6.43 g, 24 mmol), Hg(OAc)<sub>2</sub> (8.03 g, 24 mmol) and CH<sub>2</sub>Cl<sub>2</sub> (50 mL) were mixed and stirred for 24 h. Then the reaction mixture was filtered and washed with Na<sub>2</sub>S<sub>2</sub>O<sub>3</sub>, water, brine, and dried over MgSO<sub>4</sub>. The solvent was removed under vacuum. The crude product was recrystallized from EtOH to afford the compound **56** as white solid (4.55 g, 9 mmol, 71%). <sup>1</sup>H NMR (500 MHz, CDCl<sub>3</sub>): δ 7.17 (s, 2H), 3.93 (t, *J* = 6.44 Hz, 4H), 1.85-1.76 (m, 4H), 1.51-1.33 (m, 8H), 0.94 (t, *J* = 6.79 Hz, 6H). The <sup>1</sup>H NMR data is consistent with those reported in the literature.<sup>60</sup>

#### 1,4-Bis(decyloxy)-2-iodo-5-(trimethylsilylethynyl)benzene (**57**)<sup>62</sup>

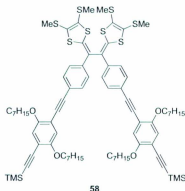


**57**

A mixture of **48** (11.18 g, 22 mmol), Pd(PPh<sub>3</sub>)<sub>2</sub>Cl<sub>2</sub> (1.5 g, 2.2 mmol), and CuI (1.26 g, 6.6 mmol) were added to 400 mL of Et<sub>3</sub>N. Then TMSA (1.956 mL, 13 mmol) was added dropwise. The reaction mixture was then stirred at 60 °C for 24 h. The resulting mixture was filtered and the filtrate was washed with NH<sub>4</sub>Cl, H<sub>2</sub>O, and brine and dried over MgSO<sub>4</sub>. The solvent was removed under vacuum. It was then subjected to column chromatography (hexanes/CH<sub>2</sub>Cl<sub>2</sub>, 9:1) to afford compound **57** (8.14 g, 13 mmol, 60%) as a colorless liquid. <sup>1</sup>H NMR (500 MHz, CDCl<sub>3</sub>): δ = 7.26 (s, 1H), 6.83 (s, 1H), 3.96-3.91

(m, 4H), 1.85-1.75 (m, 4H), 1.53-1.33 (m, 8H), 0.91-0.96 (m, 6H), 0.25 (s, 9H). The  $^1\text{H}$  NMR data is consistent with those reported in the literature.<sup>60</sup>

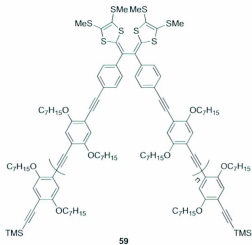
#### TTFV monomer (**58**)



To a solution of TTFV **46** (255 mg, 0.34 mmol) in THF/MeOH (16 mL, 1:1) was added  $\text{K}_2\text{CO}_3$  (260 mg, 2.04 mmol). The mixture was stirred for 0.5 h at room temperature, and it was then diluted with  $\text{CH}_2\text{Cl}_2$ , washed with  $\text{H}_2\text{O}$ , dried over  $\text{MgSO}_4$ , and concentrated *in vacuo*. To the residue was added  $\text{Et}_3\text{N}$  (50 mL) and iodoarene **54** (900 mg, 1.7 mmol). The mixture was degassed by vigorous  $\text{N}_2$  bubbling. To the mixture was then added  $\text{CuI}$  (19 mg, 0.102 mmol) and  $\text{Pd}(\text{PPh})_4$  (39 mg, 0.034 mmol). The mixture was heated at  $60^\circ\text{C}$  and kept stirring overnight. The resulting reaction mixture was diluted with  $\text{CH}_2\text{Cl}_2$ , washed sequentially with aq.  $\text{NH}_4\text{Cl}$  and  $\text{H}_2\text{O}$ , dried over  $\text{MgSO}_4$ , and concentrated *in vacuo*. The residue was purified by silica column chromatography ( $\text{CH}_2\text{Cl}_2$ /hexanes 5:95) to yield TTFV monomer **58** (297 mg, 210  $\mu\text{mol}$ , 62%) as a yellow oil.  $^1\text{H}$  NMR (500

MHz, CDCl<sub>3</sub>)  $\delta$  7.46 (d,  $J$  = 8.6 Hz, 4H), 7.38 (d,  $J$  = 8.6 Hz, 4H), 6.92 (d,  $J$  = 2.63 Hz, 4H), 4.00–3.93 (m, 8H), 2.37 (d,  $J$  = 14.6 Hz, 12H), 1.84 – 1.74 (m, 8H), 1.54 – 1.46 (m, 8H), 1.37–1.24 (m, 26H), 0.90 (m, 12H), 0.25 (s, 18H); <sup>13</sup>C NMR (75 MHz, CDCl<sub>3</sub>)  $\delta$  154.18, 153.48, 137.92, 136.63, 131.87, 128.75, 126.29, 125.09, 123.63, 121.50, 117.29, 116.84, 114.32, 113.66, 101.21, 100.06, 69.58, 69.50, 31.86, 29.72, 29.38, 29.35, 29.11, 29.07, 26.01, 22.66, 22.65, 18.95, 18.86, 14.18, 14.13; FTIR (neat) 2920, 2851, 2150, 1500, 1463, 1378, 1275, 1212, 1020 cm<sup>-1</sup>; HR–MALDI–TOF MS  $m/z$  calcd for C<sub>78</sub>H<sub>102</sub>O<sub>4</sub>S<sub>8</sub>Si<sub>2</sub> 1414.5082, found 1414.5084.

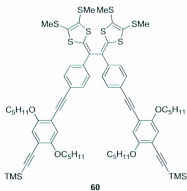
#### TTFV polymer (**59**)



To a solution of TTFV monomer **50** (123 mg, 0.087 mmol) in THF/MeOH (20 mL, 1:1) was added K<sub>2</sub>CO<sub>3</sub> (72 mg, 0.524 mmol). The mixture was stirred at room temperature for

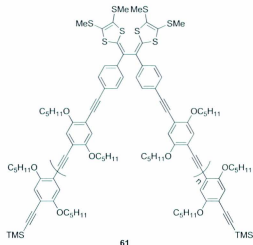
0.5 h, diluted with  $\text{CH}_2\text{Cl}_2$ , washed with  $\text{H}_2\text{O}$ , dried over  $\text{MgSO}_4$ , and concentrated *in vacuo*. To the residue was added toluene (6 mL),  $\text{CuI}$  (5 mg, 0.026 mmol),  $\text{PdCl}_2(\text{PPh})_2$  (6 mg, 0.009 mmol) and DBU (0.001 mL, 0.009 mmol). The mixture was heated at 70 °C under stirring for 1 h. Then iodoarene **54** (2 mg, 0.004 mmol) was added and the mixture was stirred for 36 h. Afterwards, methanol was added and the resulting precipitates were collected by filtration to afford TTFV polymer **59** (105mg, 92%)  $^1\text{H}$  NMR (500 MHz,  $\text{CDCl}_3$ )  $\delta$  7.46 (d,  $J = 7.5$  Hz, 60H), 7.38 (d,  $J = 7.5$ Hz, 60H), 6.98 – 6.94 (m, 60H), 4.02 – 3.96 (m, 129H), 2.44 (d,  $J = 7.5$ Hz 180H), 1.82 – 1.81(m, 135H), 1.51 – 1.26 (m, 600H), 0.87 – 0.81 (m, 234H), 0.26 (s, 18H); FTIR (neat) 2920, 2855, 2205, 1600, 1463, 1419, 1378, 1269, 1211, 1018  $\text{cm}^{-1}$ ; FTIR (neat) 2921, 2857, 2206, 1600, 1463, 1420, 1378, 1269, 1211, 1018  $\text{cm}^{-1}$ .

#### TTFV monomer (**60**)



To a solution of TTFV **46** (276 mg, 0.36 mmol) in THF/MeOH (12 mL, 1:1) was added  $K_2CO_3$  (320 mg, 2.19 mmol). The mixture was stirred for 0.5 h at room temperature, diluted with  $CH_2Cl_2$ , washed with  $H_2O$ , dried over  $MgSO_4$ , and concentrated *in vacuo*. To the residue was added  $Et_3N$  (60 mL) and iodoarene **57** (1.05 mg, 1.8 mmol). The mixture was degassed by vigorous  $N_2$  bubbling. To the mixture was then added  $CuI$  (25 mg, 0.108 mmol) and  $Pd(PPh)_4$  (51 mg, 0.036 mmol). The mixture was heated at 60 °C and kept stirring overnight. The resulting reaction mixture was diluted with  $CH_2Cl_2$ , washed sequentially with aq.  $NH_4Cl$  and  $H_2O$ , dried over  $MgSO_4$ , and concentrated *in vacuo*. The residue was purified by silica column chromatography ( $CH_2Cl_2$ /hexanes 5:95) to yield TTFV monomer **60** (309 mg, 237  $\mu$ mol, 65%) as a yellow oil.  $^1H$  NMR (500 MHz,  $CDCl_3$ )  $\delta$  7.45 (d,  $J = 8.9$  Hz, 4H), 7.37 (d,  $J = 8.9$  Hz, 4H), 6.93 (d,  $J = 2.3$  Hz, 4H), 4.00–3.95 (m, 8H), 2.38 (d,  $J = 14.5$  Hz, 12H), 1.87–1.76 (m, 8H), 1.55–1.33 (m, 18H), 0.96–0.85 (m, 14H), 0.86 (m, 12H), 0.26 (s, 18H);  $^{13}C$  NMR (75 MHz,  $CDCl_3$ )  $\delta$  154.19, 153.47, 137.91, 136.67, 131.86, 128.70, 126.34, 125.11, 123.65, 121.52, 117.30, 116.82, 114.32, 113.66, 101.21, 100.07, 95.03, 86.77, 69.50, 69.50, 29.06, 28.26, 28.22, 22.52, 22.48, 18.96, 18.86, 14.13, 14.11; FTIR (neat) 2926, 2863, 2149, 1500, 1415, 1378, 1261, 1211, 1012  $cm^{-1}$ ; HR–MALDI–TOF MS  $m/z$  calcd for  $C_{70}H_{86}O_4S_4Si_2$  1302.3830, found 1302.3806.

#### **TTFV polymer (61)**



To a solution of TTFV monomer **60** (318 mg, 0.24 mmol) in THF/MeOH (20 mL, 1:1) was added  $K_2CO_3$  (202 mg, 1.46 mmol). The mixture was stirred at room temperature for 0.5 h, and then it was diluted with  $CH_2Cl_2$ , washed with  $H_2O$ , dried over  $MgSO_4$ , and concentrated *in vacuo*. To the residue was added toluene (10 mL), CuI (13 mg, 0.072 mmol),  $PdCl_2(PPh)_2$  (16 mg, 0.024 mmol) and DBU (0.004 mL, 0.024 mmol). The mixture was heated at 70 °C under stirring for 1 h. Then iodoarene **57** (5 mg, 0.012 mmol) was added and the mixture was stirred for 36 h. Afterwards, methanol was added and the resulting precipitates were collected by filtration to afford TTFV polymer **61** (260 mg, 90%)  $^1H$  NMR (500 MHz,  $CDCl_3$ )  $\delta$  7.48 (d,  $J = 8.1$  Hz, 76H), 7.40 (d,  $J = 8.0$  Hz, 76H), 6.97 (m, 76H), 4.03 – 3.96 (m, 160H), 2.44 – 2.36 (m, 255H), 1.88 – 1.79 (m, 168H), 1.53 – 1.37 (m, 361H), 0.97 – 0.90 (m, 260H), 0.07 (s, 18H); FTIR (neat) 2920, 2855, 2205, 1600, 1463, 1419, 1378, 1269, 1211, 1018  $cm^{-1}$ .

## Chapter 4

### Conclusions and Future Work

This thesis work aims at the development of TTFV-based conjugate polymers to reversibly disperse and release SWNTs in a controlled manner. In the first project, a TTFV-based phenylacetylene conjugated polymer **51** was synthesized and characterized to demonstrate that TTFV can serve as an effective switching unit to impart the polymer with redox-controlled conformational switching behavior. Moreover, the supramolecular interactions between TTFV-phenylacetylene foldamer **51** and SWNTs have been found to be tube diameter-dependent. The wrapping mode facilitates the dispersion of individual small-diameter tubes, giving stable and organic soluble SWNT-polymer assemblies, while the adhesion mode works for large-diameter tubes to form supramolecular networks and produce appealing SWNT/polymer sol-gels. Finally, Polymer **51** is responsive to external stimuli (redox and acidity) to allow for reversible dispersion and releasing of SWNTs in solution, which opens a new avenue for developing cost-effective methods, such as continuous flow, to enrich or purify specific types of SWNTs.

In the second project, two analogous TTFV-based conjugated polymers **59** and **61** with different side chains have been synthesized and characterized. Comparative studies of the TTFV polymers show that the side chains have little effect on the redox properties of the

TTFV polymers. TTFV polymers **59** and **61** also can also disperse SWNTs in organic solvents, giving stable and organic soluble SWNT-polymer assemblies. Studies of the side-chain effect reveal that the side chains of polymers prefer to interact with larger-diameter tubes via alkyl- $\pi$  interactions, while the wrapping of the TTFV polymers is more selective towards smaller-diameter tubes. As a conclusion, TTFV polymers with shorter side chains have better selectivity for small-diameter SWNTs. However, the good selectivity is at the expense of lowered solubility. To improve this, future work should be focused on the preparation of polymers with short but bulky side chains.

## Bibliography

1. Iijima, S., Helical microtubules of graphitic carbon. *Nature* **1991**, *354* (6348), 56-58.
2. Byrne, M. T.; Gun'ko, Y. K., Recent Advances in Research on Carbon Nanotube–Polymer Composites. *Adv. Mater.* **2010**, *22* (15), 1672-1688.
3. Yu, M.-F.; Lourie, O.; Dyer, M. J.; Moloni, K.; Kelly, T. F.; Ruoff, R. S., Strength and Breaking Mechanism of Multiwalled Carbon Nanotubes Under Tensile Load. *Science* **2000**, *287* (5453), 637-640.
4. Yu, M.-F.; Files, B. S.; Arepalli, S.; Ruoff, R. S., Tensile Loading of Ropes of Single Wall Carbon Nanotubes and their Mechanical Properties. *Phys. Rev. Lett.* **2000**, *84* (24), 5552-5555.
5. Frank, S.; Poncharal, P.; Wang, Z. L.; Heer, W. A. d., Carbon Nanotube Quantum Resistors. *Science* **1998**, *280* (5370), 1744-1746.
6. Liu, Z.; Jiao, L.; Yao, Y.; Xian, X.; Zhang, J., Aligned, Ultralong Single-Walled Carbon Nanotubes: From Synthesis, Sorting, to Electronic Devices. *Adv. Mater.* **2010**, *22* (21), 2285-2310.
7. Dai, H.; Javey, A.; Pop, E.; Mann, D.; Kim, W.; Lu, Y., Electrical Transport Properties and Field Effect Transistors of Carbon Nanotubes. *Nano* **2006**, *01* (01), 1-13.
8. Hirsch, A., Functionalization of Single-Walled Carbon Nanotubes. *Angew. Chem. Int. Ed.* **2002**, *41* (11), 1853-1859.
9. Rao, C. N. R.; Satishkumar, B. C.; Govindaraj, A.; Nath, M., Nanotubes. *ChemPhysChem* **2001**, *2* (2), 78-105.

10. Nikolaev, P.; Bronikowski, M. J.; Bradley, R. K.; Rohmund, F.; Colbert, D. T.; Smith, K. A.; Smalley, R. E., Gas-Phase Catalytic Growth of Single-Walled Carbon Nanotubes from Carbon Monoxide. *Chem. Phys. Lett.* **1999**, *313* (1–2), 91–97.
11. Saito, R.; Fujita, M.; Dresselhaus, G.; Dresselhaus, M. S., Electronic Structure of Chiral Graphene Tubules. *Appl. Phys. Lett.* **1992**, *60* (18), 2204–2206.
12. Tchoul, M. N.; Ford, W. T.; Lolli, G.; Resasco, D. E.; Arepalli, S., Effect of Mild Nitric Acid Oxidation on Dispersability, Size, and Structure of Single-Walled Carbon Nanotubes. *Chem. Mater.* **2007**, *19* (23), 5765–5772.
13. Liu, J.; Rinzler, A. G.; Dai, H.; Hafner, J. H.; Bradley, R. K.; Boul, P. J.; Lu, A.; Iverson, T.; Shelimov, K.; Huffman, C. B.; Rodriguez-Macias, F.; Shon, Y.-S.; Lee, T. R.; Colbert, D. T.; Smalley, R. E., Fullerene Pipes. *Science* **1998**, *280* (5367), 1253–1256.
14. Peng, X.; Wong, S. S., Functional Covalent Chemistry of Carbon Nanotube Surfaces. *Adv. Mater.* **2009**, *21* (6), 625–642.
15. Herranz, M. Á.; Martín, N.; Campidelli, S.; Prato, M.; Brehm, G.; Guldi, D. M., Control over Electron Transfer in Tetrathiafulvalene-Modified Single-Walled Carbon Nanotubes. *Angew. Chem. Int. Ed.* **2006**, *45* (27), 4478–4482.
16. O'Connell, M. J.; Bachilo, S. M.; Huffman, C. B.; Moore, V. C.; Strano, M. S.; Haroz, E. H.; Rialon, K. L.; Boul, P. J.; Noon, W. H.; Kittrell, C.; Ma, J.; Hauge, R. H.; Weisman, R. B.; Smalley, R. E., Band Gap Fluorescence from Individual Single-Walled Carbon Nanotubes. *Science* **2002**, *297* (5581), 593–596.

17. Chen, R. J.; Zhang, Y.; Wang, D.; Dai, H., Noncovalent Sidewall Functionalization of Single-Walled Carbon Nanotubes for Protein Immobilization. *J. Am. Chem. Soc.* **2001**, *123* (16), 3838-3839.
18. Nakashima, N.; Tomonari, Y.; Murakami, H., Water-Soluble Single-Walled Carbon Nanotubes via Noncovalent Sidewall-Functionalization with a Pyrene-Carrying Ammonium Ion. *Chem. Lett.* **2002**, *31* (6), 638-639.
19. Matsuzawa, Y.; Kato, H.; Ohyama, H.; Nishide, D.; Kataura, H.; Yoshida, M., Photoinduced Dispersibility Tuning of Carbon Nanotubes by a Water-Soluble Stilbene as a Dispersant. *Adv. Mater.* **2011**, *23* (34), 3922-3925.
20. Li, H.; Zhou, B.; Lin, Y.; Gu, L.; Wang, W.; Fernando, K. A. S.; Kumar, S.; Allard, L. F.; Sun, Y.-P., Selective Interactions of Porphyrins with Semiconducting Single-Walled Carbon Nanotubes. *J. Am. Chem. Soc.* **2004**, *126* (4), 1014-1015.
21. Nobusawa, K.; Ikeda, A.; Kikuchi, J.-i.; Kawano, S.-i.; Fujita, N.; Shinkai, S., Reversible Solubilization and Precipitation of Carbon Nanotubes through Oxidation-Reduction Reactions of a Solubilizing Agent. *Angew. Chem. Int. Ed.* **2008**, *47* (24), 4577-4580.
22. Star, A.; Stoddart, J. F.; Steuerman, D.; Diehl, M.; Boukai, A.; Wong, E. W.; Yang, X.; Chung, S.-W.; Choi, H.; Heath, J. R., Preparation and Properties of Polymer-Wrapped Single-Walled Carbon Nanotubes. *Angew. Chem. Int. Ed.* **2001**, *40* (9), 1721-1725.
23. Steuerman, D. W.; Star, A.; Narizzano, R.; Choi, H.; Ries, R. S.; Nicolini, C.; Stoddart, J. F.; Heath, J. R., Interactions between Conjugated Polymers and Single-Walled Carbon Nanotubes. *J. Phys. Chem. B* **2002**, *106* (12), 3124-3130.

24. Star, A.; Liu, Y.; Grant, K.; Ridvan, L.; Stoddart, J. F.; Steurman, D. W.; Diehl, M. R.; Boukai, A.; Heath, J. R., Noncovalent Side-Wall Functionalization of Single-Walled Carbon Nanotubes. *Macromolecules* **2003**, *36* (3), 553-560.
25. Zhao, Y.-L.; Stoddart, J. F., Noncovalent Functionalization of Single-Walled Carbon Nanotubes. *Acc. Chem. Res.* **2009**, *42* (8), 1161-1171.
26. Shigetani, M. K., Masaharu Nakashima, Naotoshi, Individual Solubilization of Single-Walled Carbon Nanotubes Using Totally Aromatic Polyimide. *Chem. Phys. Lett.* **2006**, *418* (1-3), 115-118.
27. Nakayama-Ratchford, N.; Bangsaruntip, S.; Sun, X.; Welsher, K.; Dai, H., Noncovalent Functionalization of Carbon Nanotubes by Fluorescein-Polyethylene Glycol: Supramolecular Conjugates with pH-Dependent Absorbance and Fluorescence. *J. Am. Chem. Soc.* **2007**, *129* (9), 2448-2449.
28. Lee, H. W.; Yoon, Y.; Park, S.; Oh, J. H.; Hong, S.; Liyanage, L. S.; Wang, H.; Morishita, S.; Patil, N.; Park, Y. J.; Park, J. J.; Spakowitz, A.; Galli, G.; Gygi, F.; Wong, P. H. S.; Tok, J. B. H.; Kim, J. M.; Bao, Z., Selective Dispersion of High Purity Semiconducting Single-Walled Carbon Nanotubes with Regioregular Poly(3-alkylthiophene)s. *Nat. Commun.* **2011**, *2*, 541.
29. Nish, A.; Hwang, J.-Y.; Doig, J.; Nicholas, R. J., Highly Selective Dispersion of Single-Walled Carbon Nanotubes Using Aromatic Polymers. *Nat. Nano.* **2007**, *2* (10), 640-646.

30. Kang, Y. K.; Lee, O.-S.; Deria, P.; Kim, S. H.; Park, T.-H.; Bonnell, D. A.; Saven, J. G.; Therien, M. J., Helical Wrapping of Single-Walled Carbon Nanotubes by Water Soluble Poly(p-phenyleneethynylene). *Nano Lett.* **2009**, *9* (4), 1414-1418.
31. Chen, J.; Liu, H.; Weimer, W. A.; Halls, M. D.; Waldeck, D. H.; Walker, G. C., Noncovalent Engineering of Carbon Nanotube Surfaces by Rigid, Functional Conjugated Polymers. *J. Am. Chem. Soc.* **2002**, *124* (31), 9034-9035.
32. Rice, N. A.; Soper, K.; Zhou, N.; Merschrod, E.; Zhao, Y., Dispersing As-Prepared Single-Walled Carbon Nanotube Powders with Linear Conjugated Polymers. *Chem. Commun.* **2006**, (47), 4937-4939.
33. O'Connell, M. J.; Boul, P.; Ericson, L. M.; Huffman, C.; Wang, Y.; Haroz, E.; Kuper, C.; Tour, J.; Ausman, K. D.; Smalley, R. E., Reversible Water-Solubilization of Single-Walled Carbon Nanotubes by Polymer Wrapping. *Chem. Phys. Lett.* **2001**, *342* (3-4), 265-271.
34. Zhang, Z.; Che, Y.; Smaldone, R. A.; Xu, M.; Bunes, B. R.; Moore, J. S.; Zang, L., Reversible Dispersion and Release of Carbon Nanotubes Using Foldable Oligomers. *J. Am. Chem. Soc.* **2010**, *132* (40), 14113-14117.
35. Wang, D.; Chen, L., Temperature and pH-Responsive Single-Walled Carbon Nanotube Dispersions. *Nano Lett.* **2007**, *7* (6), 1480-1484.
36. Chen, S.; Jiang, Y.; Wang, Z.; Zhang, X.; Dai, L.; Smet, M., Light-Controlled Single-Walled Carbon Nanotube Dispersions in Aqueous Solution. *Langmuir* **2008**, *24* (17), 9233-9236.

37. Zou, J.; Liu, L.; Chen, H.; Khondaker, S. I.; McCullough, R. D.; Huo, Q.; Zhai, L., Dispersion of Pristine Carbon Nanotubes Using Conjugated Block Copolymers. *Adv. Mater.* **2008**, *20* (11), 2055-2060.
38. Ozawa, H.; Fujigaya, T.; Niidome, Y.; Hotta, N.; Fujiki, M.; Nakashima, N., Rational Concept To Recognize/Extract Single-Walled Carbon Nanotubes with a Specific Chirality. *J. Am. Chem. Soc.* **2011**, *133* (8), 2651-2657.
39. Ju, S.-Y.; Doll, J.; Sharma, I.; Papadimitrakopoulos, F., Selection of carbon nanotubes with specific chiralities using helical assemblies of flavin mononucleotide. *Nat. Nano* **2008**, *3* (6), 356-362.
40. Zheng, M.; Jagota, A.; Semke, E. D.; Diner, B. A.; McLean, R. S.; Lustig, S. R.; Richardson, R. E.; Tassi, N. G., DNA-assisted dispersion and separation of carbon nanotubes. *Nat. Mater.* **2003**, *2* (5), 338-342.
41. Dieckmann, G. R.; Dalton, A. B.; Johnson, P. A.; Razal, J.; Chen, J.; Giordano, G. M.; Muñoz, E.; Musselman, I. H.; Baughman, R. H.; Draper, R. K., Controlled Assembly of Carbon Nanotubes by Designed Amphiphilic Peptide Helices. *J. Am. Chem. Soc.* **2003**, *125* (7), 1770-1777.
42. Zhao, Y.; Chen, G.; Mulla, K.; Mahmud, I.; Liang, S.; Dongare, P.; Thompson, D. W.; Dawe, L. N.; Bouzan, S., Tetrathiafulvalene Vinyllogues as Versatile Building Blocks for New Organic Materials. *Pure Appl. Chem.* **2012**, *84* (4), 1005-1025.
43. Carlier, R.; Hapiot, P.; Lorey, D.; Robert, A.; Tallec, A., Electrosynthesis and Redox Behavior of Vinyllogous TTF Displaying Strong Conformational Changes Associated with Electron Transfers. *Electrochimica Acta* **2001**, *46* (20-21), 3269-3277.

44. A. Jorio, G. D. a. M. S. D., Carbon Nanotubes: Advanced Topics in the Synthesis, Structure, Properties and Application. Springer: Berlin 2008.
45. Britz, D. A.; Khlobystov, A. N., Noncovalent Interactions of Molecules with Single Walled Carbon Nanotubes. *Chem. Soc. Rev.* **2006**, 35 (7), 637-659.
46. Cathcart, H.; Nicolosi, V.; Hughes, J. M.; Blau, W. J.; Kelly, J. M.; Quinn, S. J.; Coleman, J. N., Ordered DNA Wrapping Switches on Luminescence in Single-Walled Nanotube Dispersions. *J. Am. Chem. Soc.* **2008**, 130 (38), 12734-12744.
47. Liang, S.; Chen, G.; Peddle, J.; Zhao, Y., Reversible Dispersion and Releasing of Single-Walled Carbon Nanotubes by A Stimuli-Responsive TTFV-Phenylacetylene Polymer. *Chem. Commun.* **2012**, 48 (25), 3100-2.
48. Chen, G.; Mahmud, I.; Dawe, L. N.; Zhao, Y., Acetylenic Phenylthiafulvene: A Versatile Synthon for TTFV-Based Macromolecules. *Org. Lett.* **2010**, 12 (4), 704-707.
49. Feng, J.; Alam, S. M.; Yan, L. Y.; Li, C. M.; Judeh, Z.; Chen, Y.; Li, L.-J.; Lim, K. H.; Chan-Park, M. B., Sorting of Single-Walled Carbon Nanotubes Based on Metallicity by Selective Precipitation with Polyvinylpyrrolidone. *J. Phys. Chem. C* **2011**, 115 (13), 5199-5206.
50. Hennrich, F.; Krupke, R.; Lebedkin, S.; Arnold, K.; Fischer, R.; Resasco, D. E.; Kappes, M. M., Raman Spectroscopy of Individual Single-Walled Carbon Nanotubes from Various Sources. *J. Phys. Chem. B* **2005**, 109 (21), 10567-10573.
51. Tanaka, T.; Jin, H.; Miyata, Y.; Fujii, S.; Suga, H.; Naitoh, Y.; Minari, T.; Miyadera, T.; Tsukagoshi, K.; Kataura, H., Simple and Scalable Gel-Based Separation of Metallic and Semiconducting Carbon Nanotubes. *Nano Lett.* **2009**, 9 (4), 1497-1500.

52. Tu, X.; Manohar, S.; Jagota, A.; Zheng, M., DNA sequence motifs for structure-specific recognition and separation of carbon nanotubes. *Nature* **2009**, *460* (7252), 250-253.
53. Bachilo, S. M.; Strano, M. S.; Kittrell, C.; Hauge, R. H.; Smalley, R. E.; Weisman, R. B., Structure-Assigned Optical Spectra of Single-Walled Carbon Nanotubes. *Science* **2002**, *298* (5602), 2361-2366.
54. Maeda, Y.; Kanda, M.; Hashimoto, M.; Hasegawa, T.; Kimura, S.-i.; Lian, Y.; Wakahara, T.; Akasaka, T.; Kazaoui, S.; Minami, N.; Okazaki, T.; Hayamizu, Y.; Hata, K.; Lu, J.; Nagase, S., Dispersion and Separation of Small-Diameter Single-Walled Carbon Nanotubes. *J. Am. Chem. Soc.* **2006**, *128* (37), 12239-12242.
55. Ogoshi, T.; Takashima, Y.; Yamaguchi, H.; Harada, A., Chemically-Responsive Sol-Gel Transition of Supramolecular Single-Walled Carbon Nanotubes (SWNTs) Hydrogel Made by Hybrids of SWNTs and Cyclodextrins. *J. Am. Chem. Soc.* **2007**, *129* (16), 4878-4879.
56. Chen, G. Synthesis and Electronic Properties of TTFBQ Based Donor-Acceptor Molecular Systems. Memorial University of Newfoundland, St. John's, 2006.
57. Yang, X.; Li, Z.; Zhi, J.; Ma, J.; Hu, A., Synthesis of Ultrathin Mesoporous Carbon through Bergman Cyclization of Eneidyne Self-Assembled Monolayers in SBA-15. *Langmuir* **2010**, *26* (13), 11244-11248.
58. Moy, C. L.; Kaliappan, R.; McNeil, A. J., Aryl Trihydroxyborate Salts: Thermally Unstable Species with Unusual Gelation Abilities. *J. Org. Chem.* **2011**, *76* (20), 8501-8507.

59. Bao, Z.; Chen, Y.; Cai, R.; Yu, L., Conjugated liquid-crystalline polymers - soluble and fusible poly(phenylenevinylene) by the Heck coupling reaction. *Macromolecules* **1993**, *26* (20), 5281-5286.
60. Schaate, A.; Roy, P.; Preuße, T.; Lohmeier, S. J.; Godt, A.; Behrens, P., Porous Interpenetrated Zirconium–Organic Frameworks (PIZOFs): A Chemically Versatile Family of Metal–Organic Frameworks. *Chem. Eur. J.* **2011**, *17* (34), 9320-9325.

## Appendix

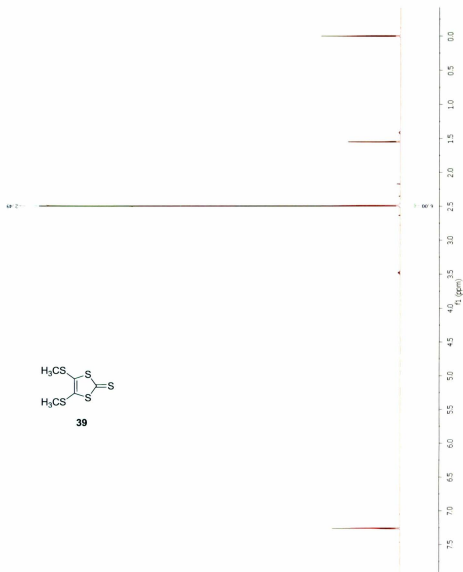


Figure A-1.  $^1\text{H}$  NMR (500 MHz,  $\text{CDCl}_3$ ) spectrum of compound **39**.

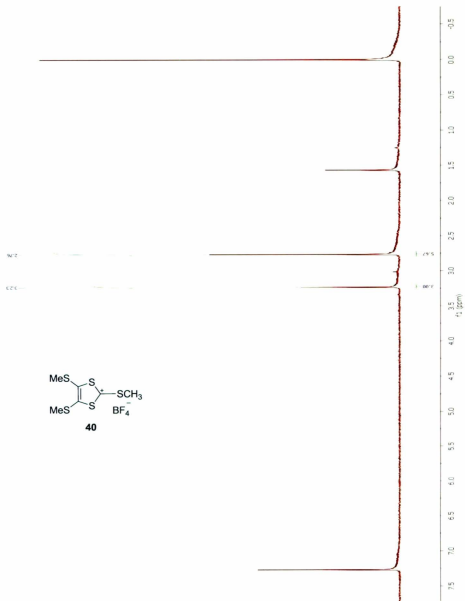


Figure A-2.  $^1\text{H NMR}$  (300 MHz,  $\text{CDCl}_3$ ) spectrum of compound **40**.

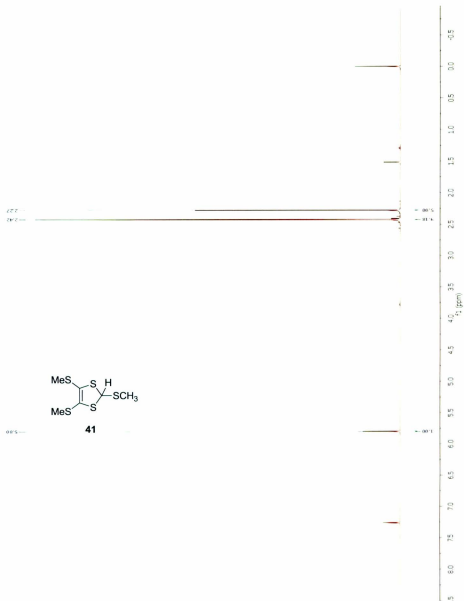


Figure A-3. <sup>1</sup>H NMR (300 MHz, CDCl<sub>3</sub>) spectrum of compound **41**.

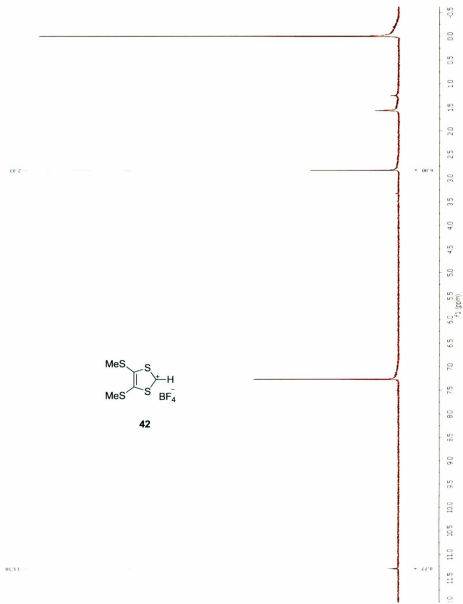


Figure A-4.  $^1\text{H}$  NMR (300 MHz,  $\text{CDCl}_3$ ) spectrum of compound **42**.

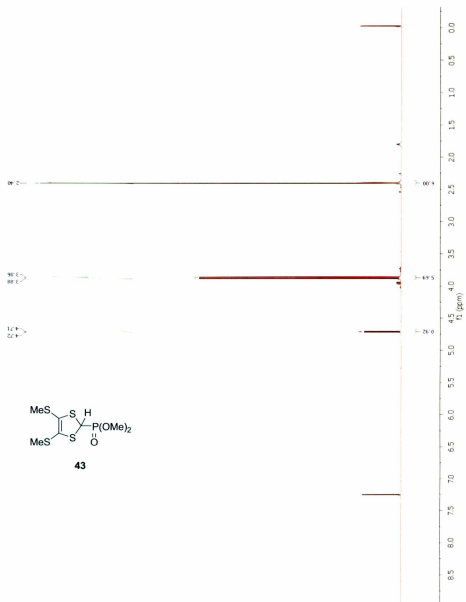


Figure A-5. <sup>1</sup>H NMR (500 MHz, CDCl<sub>3</sub>) spectrum of compound **43**.

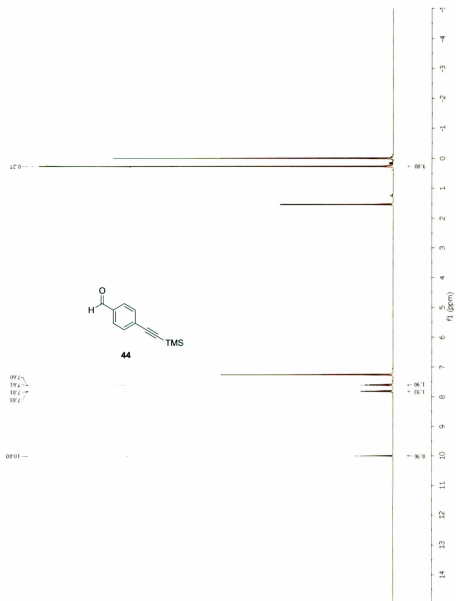


Figure A-6. <sup>1</sup>H NMR (500 MHz, CDCl<sub>3</sub>) spectrum of compound **44**.

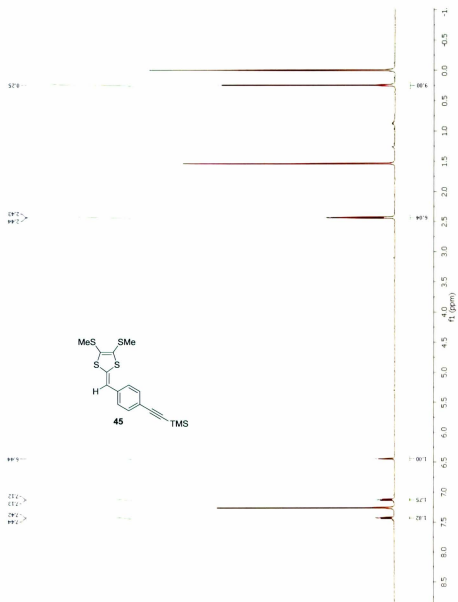
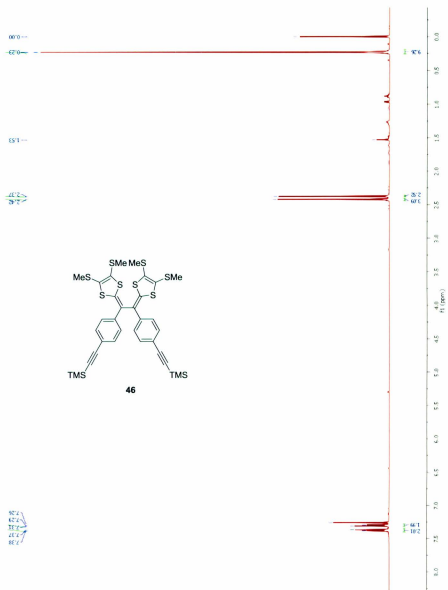


Figure A-7.  $^1\text{H NMR}$  (500 MHz,  $\text{CDCl}_3$ ) spectrum of compound **45**.



**Figure A-8.**  $^1\text{H}$  NMR (500 MHz,  $\text{CDCl}_3$ ) spectrum of compound **46**.

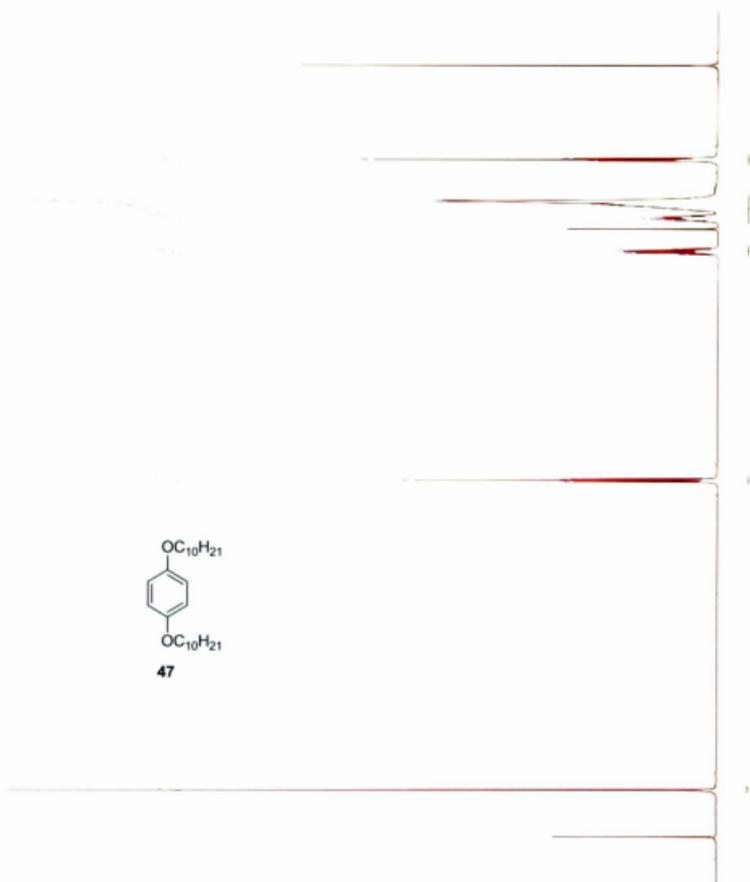


Figure A-9. <sup>1</sup>H NMR (300 MHz, CDCl<sub>3</sub>) spectrum of compound 47.

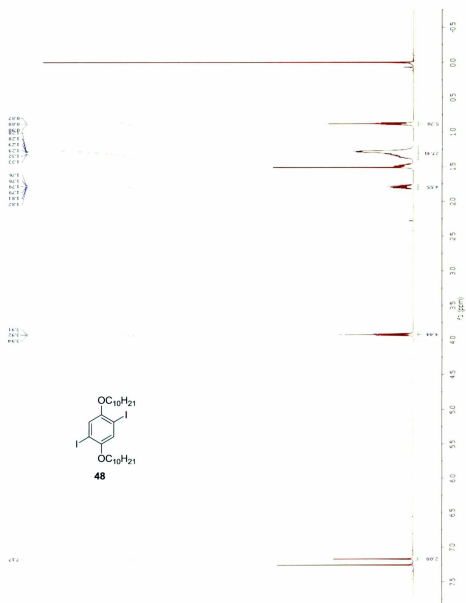


Figure A-10.  $^1\text{H}$  NMR (500 MHz,  $\text{CDCl}_3$ ) spectrum of compound **48**.

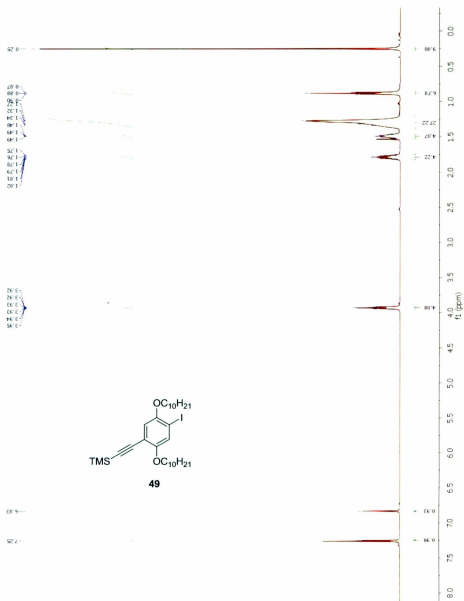


Figure A-11. <sup>1</sup>H NMR (500 MHz, CDCl<sub>3</sub>) spectrum of compound **49**.

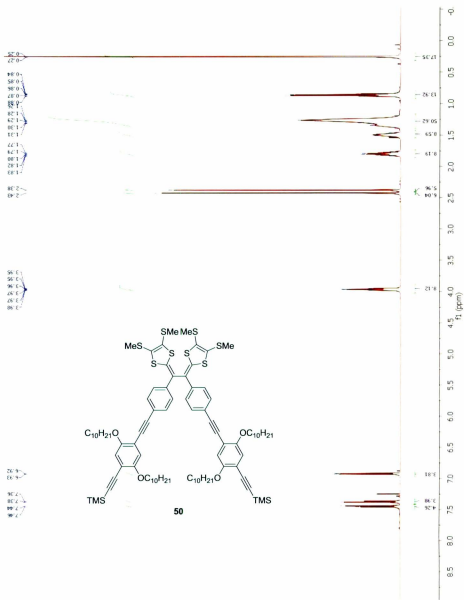


Figure A-12. <sup>1</sup>H NMR (500 MHz, CDCl<sub>3</sub>) spectrum of compound 50.



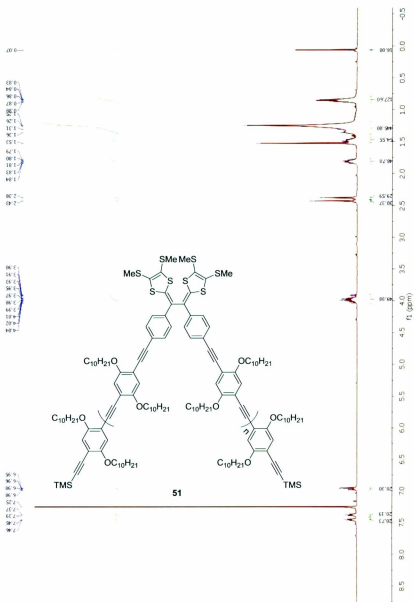


Figure A-14.  $^1\text{H}$  NMR (500 MHz,  $\text{CDCl}_3$ ) spectrum of compound **51**.



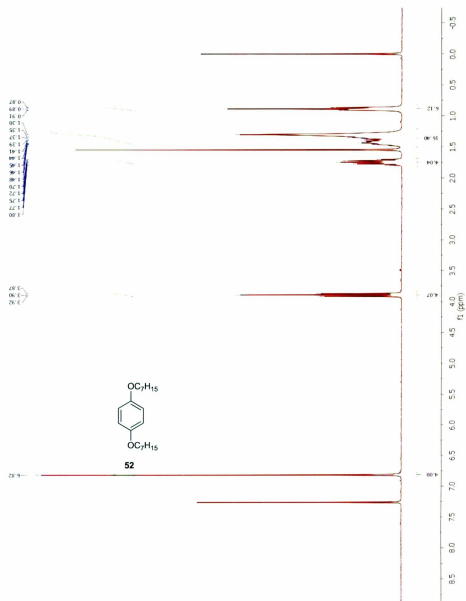


Figure A-16.  $^1\text{H}$  NMR (300 MHz,  $\text{CDCl}_3$ ) spectrum of compound **52**.

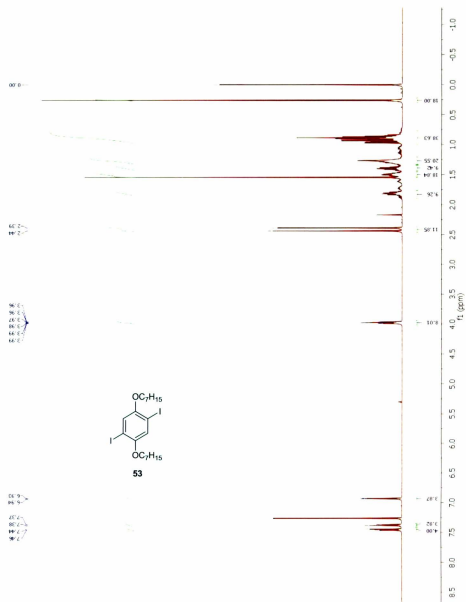


Figure A-17.  $^1\text{H}$  NMR (500 MHz,  $\text{CDCl}_3$ ) spectrum of compound **53**.

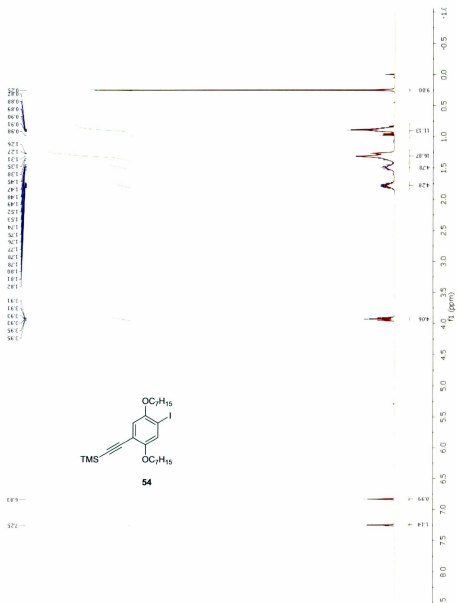


Figure A-18. <sup>1</sup>H NMR (500 MHz, CDCl<sub>3</sub>) spectrum of compound **54**.

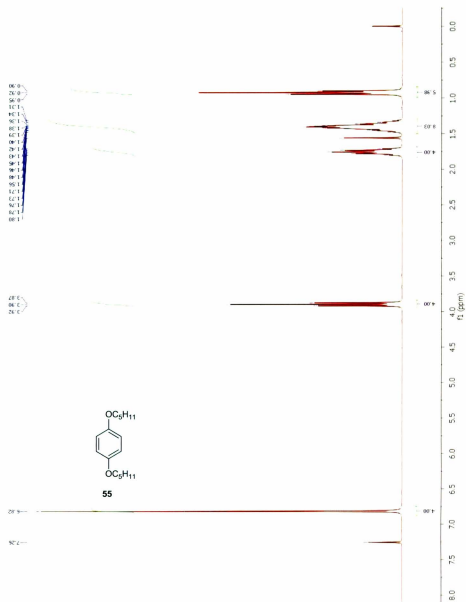


Figure A-19.  $^1\text{H}$  NMR (300 MHz,  $\text{CDCl}_3$ ) spectrum of compound **55**.



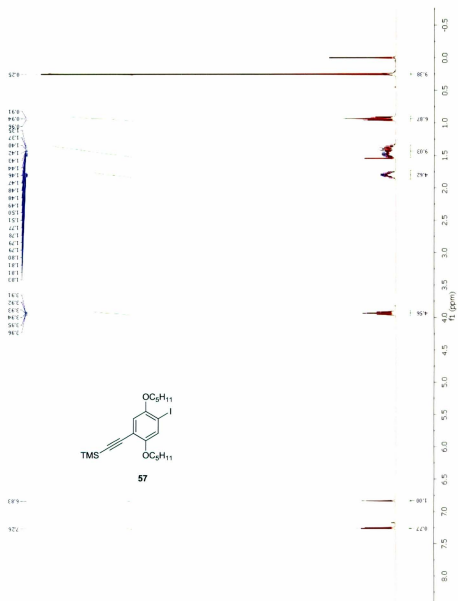


Figure A-21. <sup>1</sup>H NMR (500 MHz, CDCl<sub>3</sub>) spectrum of compound **57**.

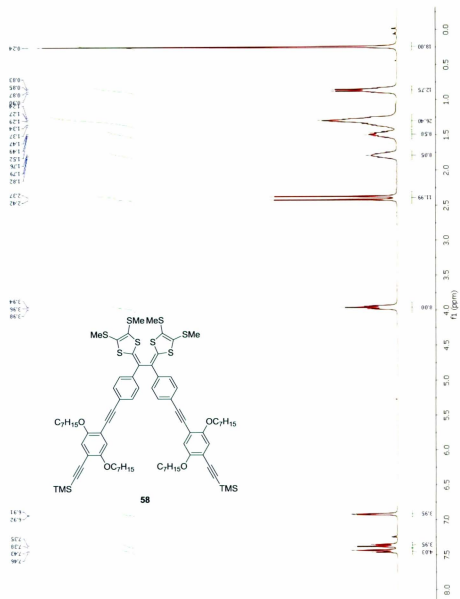


Figure A-22.  $^1\text{H}$  NMR (500 MHz,  $\text{CDCl}_3$ ) spectrum of compound **58**.







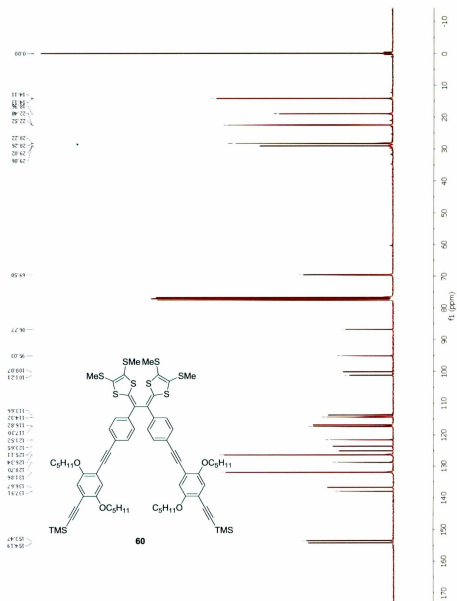


Figure A-26. <sup>13</sup>C NMR (75 MHz, CDCl<sub>3</sub>) spectrum of compound **60**.

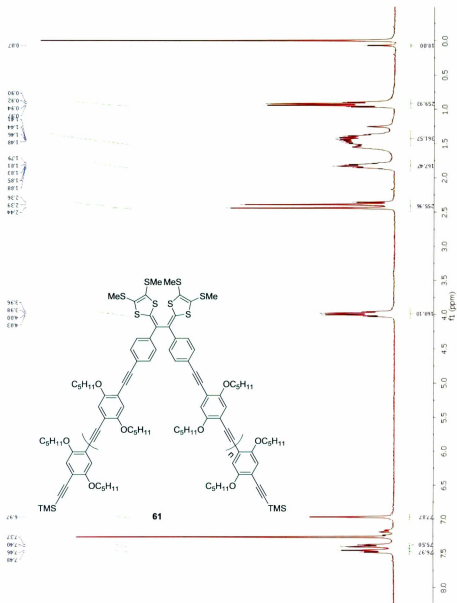


Figure A-27. <sup>1</sup>H NMR (500 MHz, CDCl<sub>3</sub>) spectrum of compound **61**.





